Dynamic self-consistent field theory for unentangled homopolymer fluids

Maja Mihajlovic
Department of Chemistry, City College, City University of New York, New York, New York 10031, USA

Tak Shing Lo
The Levich Institute, City College, City University of New York, New York, New York 10031, USA

Yitzhak Shnidman*
Department of Engineering Science and Physics, College of Staten Island, City University of New York, Staten Island, New York 10314, USA, and the NSF MRSEC for Polymers at Engineered Interfaces, Stony Brook University, Stony Brook, New York, 11794, USA

(Received 10 November 2004; revised manuscript received 4 May 2005; published 3 October 2005)

We present a lattice formulation of a dynamic self-consistent field (DSCF) theory that is capable of resolving interfacial structure, dynamics, and rheology in inhomogeneous, compressible melts and blends of unentangled homopolymer chains. The joint probability distribution of all the Kuhn segments in the fluid, interacting with adjacent segments and walls, is approximated by a product of one-body probabilities for free segments interacting solely with an external potential field that is determined self-consistently. The effect of flow on ideal chain conformations is modeled with finitely extensible, nonlinearly elastic dumbbells in the Peterlin approximation, and related to stepping probabilities in a random walk. Free segment and stepping probabilities generate statistical weights for chain conformations in a self-consistent field, and determine local volume fractions of chain segments. Flux balance across unit lattice cells yields mean field transport equations for the evolution of free segment probabilities and of momentum densities on the Kuhn length scale. Diffusive and viscous contributions to the fluxes arise from segmental hops modeled as a Markov process, with transition rates reflecting changes in segmental interaction, kinetic energy, and entropic contributions to the free energy under flow. We apply the DSCF equations to study both transient and steady-state interfacial structure, flow, and rheology in a sheared planar channel containing either a one-component melt or a phase-separated, two-component blend.

DOI: 10.1103/PhysRevE.72.041801 PACS number(s): 83.80.Tc, 83.80.Sg, 83.85.Pt, 83.50.Lh

I. INTRODUCTION

In contrast to equilibrium theories, nonequilibrium, dynamic modeling of inhomogeneous polymer fluids is still in its infancy. In such systems, the time evolution of interfacial structure, flow, and rheology is coupled to chain stretching and orientation caused by deformation under flow that is balanced by entropic restoring forces, as well as by segmental interactions. Understanding and predicting the interplay between these processes, and their dependence on composition, and on chain conformation statistics under nonuniform flow, is a challenging fundamental problem. Development of efficient computational models addressing this problem is needed for understanding and design of polymer processing, and for many other industrial and biological applications. We present here a dynamic self-consistent field (DSCF) theory that constitutes such a model, and apply it for modeling both transient and steady-state behavior of inhomogeneous fluids composed of unentangled homopolymers between sheared walls.

Our DSCF theory assumes that, on short time and length scales, liquids can be approximated by closely packed arrangements of microscopic constituents with a fluctuating distribution of free volume. In simple liquids, the microscopic constituents are atoms or compact molecules [1–4]. Similarly, unentangled polymer liquids can be viewed as freely jointed chains of Kuhn segments [5–9] that are packed into closely packed arrangements with a fluctuating distribution of free volume. We assume that at any given time, each Kuhn segment is within a cage consisting of closely packed adjacent segments, and the free volume is distributed as vacancy defects in the close-packed structure. On short time and length scales, we model such cages as Wigner-Seitz unit cells on a close-packed face-centered cubic (fcc) lattice, which are either occupied by a Kuhn segment, or are vacant. The DSCF theory attributes diffusive and viscous fluxes to segmental hops from occupied cages to adjacent vacant cages, and convective fluxes account for cage advection by the mass-averaged flow velocity. Since it is a formidable task to formulate a continuous model of such hopping events between discrete cages, we chose to use an approximate lattice description. Segmental hopping between adjacent unit cells on a lattice is modeled in our DSCF theory as a Markov process in time, with thermally activated transition rates [1–4] reflecting the changes in segmental interaction, kinetic energy, and entropic chain deformation [6,10] contributions to the self-consistent potential under flow, resulting from a single hop. By combining a kinetic mean field [11] description of the diffusive and viscous contributions to species and

*Corresponding author. Electronic address: shnidman@mail.csi.cuny.edu

momentum fluxes [3,4] with convective and elastic contributions, we obtain microscopic mean field transport equations for the time evolution of free segment probabilities and momentum densities.

A different Markov process, not to be confused with the one just mentioned above, is used as a tool for characterizing the statistics of chain conformations of jointed chains of Kuhn segments on a lattice, at any fixed moment in time [12]. In this second Markov process, all possible chain conformations are generated by a random walker stepping between adjacent lattice sites, where the steps are labeled not by time, but rather by segmental order along the generated chain (the so-called contour length variable). We reserve the term "hopping" to describe real movement of segments from one cage to another between successive moments in time, as described by the first Markov process. We use the term "stepping" to describe the placement of the next segment at an adjacent lattice site by the fictitious random walker defining the second Markov process.

Consider first a random walker that (a) has no memory of previously visited sites, (b) is isolated from any other random walkers, walls, and external potentials, and (c) does not feel any stretching or orientation constraints imposed by flow. Such a random walker has an isotropic (conditional) stepping probability to step from a site to any adjacent site on the lattice, and generates a distribution of random walks reflecting the statistics of ideal (noninteracting) jointed chains of Kuhn segments in equilibrated polymer melts [5,7]. In the equilibrium SCF lattice theory formulated by Scheutjens and Fleer [12], the interactions between the random walker at a given site, and segments and walls occupying the adjacent sites, are modeled by an effective external potential at the site occupied by the walker. In the presence of this external potential field, which is determined self-consistently, the transition rate to make the step toward an adjacent site is modified and becomes the product of the isotropic stepping probability in the absence of a potential field, and of the one-body mean field probability to find a free segment (monomer) at the adjacent site, interacting with the self-consistent potential field at that site.

The mean field approximation factorizes the joint probability for a distribution of all the Kuhn segments on the entire lattice into a product of one-body site probabilities interacting with a self-consistent potential field. It neglects pair correlations between any two segments, including the intrachain correlations between segments jointed into chains which are known to play an important role in polymer fluids. To account for intrachain correlations, the external potential field is calculated self-consistently by averaging over the interactions with walls and with other segments at neighboring sites, using not the one-body free segment probabilities at those sites, but rather the local segmental volume fractions of connected segments. The latter are calculated using the master equation governing the random walk in a self-consistent field. Near walls, and in interfacial regions between phase-separated domains of immiscible polymer blends, the segmental volume fractions of connected segments differ significantly from the one-body free segment probabilities.

If a polymer melt or blend is equilibrated in a channel between two planar walls, which are then subjected to a steady shear, momentum is transferred between the moving walls and the polymer liquid, establishing a nonuniform velocity distribution across the channel which may vary in time. Shear flow stretches and orients the chains along preferred directions, and thus modifies the statistical distribution of their end-to-end distance at any fixed moment in time. This imposes a constraint on the distribution of chain conformations generated by the random walker. The second moment of the end-to-end distance of a chain of freely jointed Kuhn segments is a symmetric second-rank tensor called the chain conformation tensor [6,8,9]. In bulk rheology of unentangled polymer melts, the simplest models for the time evolution of the chain conformation tensor in a nonuniform flow relate it to the time evolution of the second moment of the end-to-end distance of a fictitious dumbbell consisting of just two beads in a nonuniform flow, that are connected by either a harmonic, or a finitely extensible, nonlinearly elastic (FENE) spring [6,8,9], with an entropic (temperature-dependent) spring constant. The latter is tuned to reproduce the equilibrium components of the conformation tensor for ideal chains. By matching the components of the chain conformation tensor that is generated by the lattice random walk for ideal (noninteracting) test chains under flow, with the components of the chain conformation tensor obtained from the Peterlin approximation [13–18] to the FENE model (also called the FENE-P model), we are able to determine the values of the anisotropic stepping probabilities that are consistent with the stretching and orientation constraints imposed by the flow. The products of the stepping probability from the site of origin with the one-body free segment probabilities at the destination site are used as the transition rates for the Markov process generating the conformations of interacting chains as random walks in a self-consistent potential field accounting for segmental interactions.

In continuous versions of equilibrium polymer SCF theory [19–22], the Chapman-Kolmogorov integro-differential equation, rather than the discrete master equation, is the equation governing the random walk Markov process, and chain conformations are generated as continuous trajectories, rather than a sequence of discrete lattice steps. This leads to a diffusion equation for the propagation of the random walker in a self-consistent field, where the contour length variable plays the role of time. We chose to use a lattice (rather than continuum) formulation for our polymer DSCF theory because of the inherently discrete nature of the hopping dynamics between close-packed cages with fluctuating free volume, which is difficult to implement in a continuous model. Since a lattice formulation avoids functional differentiations and integrations necessary in a field-theoretical continuous formulation, it is also easier to grasp and to simulate.

The evolution equations of our DSCF lattice theory assume the form of a coupled system of nonlinear ordinary differential equations (ODEs), rather than a coupled system of nonlinear partial differential equations (PDEs), which would be the outcome of a continuous theory. This simplifies considerably the analysis, programming, and computational costs involved in numerical solutions of DSCF equations. It also facilitates comparison with molecular dynamics (MD) simulations, which are typically analyzed using averages of

densities and fluxes within discrete space-time bins. A continuous, field-theoretical formulation of our DSCF approach is conceivable, but is left for future work.

We conclude this section with an outline for the remainder of the paper. In Sec. II we briefly discuss alternate approaches for modeling the dynamics of inhomogeneous polymer fluids and their limitations. In Sec. III we present a general formulation of our DSCF theory for unentangled homopolymer fluids, resulting in a closed system of coupled time evolution equations for a set of variables defined at lattice sites. In Sec. IV we use numerical solutions of the DSCF evolution equations to study a one-component melt of unentangled homopolymer chains in a channel between two sheared planar walls. In Sec. V we use the DSCF evolution equations to study a phase-separated, two-component blend of unentangled homopolymer chains in a sheared planar channel. Section VI discusses the limitations of the current version of our DSCF approach and possible ways for generalizing and improving it.

II. ALTERNATE APPROACHES

To put our DSCF model in perspective, we discuss in this section a number of alternate approaches for modeling the dynamics of inhomogeneous polymer fluids. A weak form of dynamic SCF theories for polymer fluids was obtained by assuming that the ideal chain conformation tensor is not significantly perturbed from its equilibrium value. This neglects chain stretching and orientation by nonuniform flows and limits these methods to modeling dynamics under small perturbations from equilibrium. A local equilibrium approximation of this sort was proposed by Kawasaki and Sekimoto [23]. Fraaije [24] developed a dynamic mean field density functional method, coupled to a noisy time-dependent Landau-Ginzburg model for diffusive transport. This model was used to study microphase separation kinetics in incompressible block copolymer melts in two [24] and three [25] dimensions. Subsequent work included extension of this approach to compressible systems [26], inclusion of nonlocal kinetic coefficients [27], and addition of convective transport to the dynamics [28]. Hasegawa and Doi used a similar model to study adsorption dynamics in a polymer solution at interfaces [29] and the kinetics of a grafting reaction of end-functionalized polymers onto a solid surface [30]. Furuichi *et al.* [31] studied the conformational relaxation of a single tethered polymer chain using the dynamic mean field approach proposed by Fraaije [24], where the chemical potential is obtained using a path integral method [5]. Kawakatsu [32] derived a simplified equation of motion for the order parameter by a perturbation expansion of the distribution of chain conformations about the ideal Gaussian distribution, and applied it to investigate microphase separation in block copolymers and the effect of shear flow on ordering dynamics. Morita *et al.* used this method to study phase separation of thin polymer blend films placed between the solid substrate and free surface [33], and the competition between the micro- and macrophase separations in a binary mixture of long and short block copolymers [34]. Maurits *et al.* [35] derived an expression for the stress within the framework of the dynamic mean field density functional theory, using the principle of virtual work [5]. Viscoelastic effects were included [36] by accounting for polymer stretching and orientation in an imposed simple steady shear flow, by means of adapting the polymer configurational distribution function under flow using a dumbbell model [6].

Most recently, Shima *et al.* [37] proposed combining the continuous SCF approach with a reptation model to account for deformations of chain conformations in inhomogeneous *entangled* polymer fluids under strong shearing flows. They validated the model by comparison with the predictions of the reptation theory for homogeneous shearing flows, and then applied it to study polymer brushes grafted to walls that are sheared apart at a constant shear rate. Their theory models the time evolution of the orientation of *reptation tube segments*, whose characteristic length is the tube diameter, which is significantly larger than the Kuhn length. They derive a drift-diffusion equation for the statistical weight of the conformations of a connected chain of reptation tube segments in a self-consistent field, where the tube contour length plays the role of time. They relate the "drift velocity" and the "diffusion" coefficient in this equation to the first and second moments of the probability distribution of the local tangent vectors to the tube, which evolves according to a transport equation based on reptation theory. The second moment is also related to the stress. Thus the evolution equations for the first and second moments of the local tangent vectors play a role similar to that of the FENE-P dumbbell model in our DSCF theory for unentangled polymer fluids, which "guides" the evolution of our stepping probabilities, which become anisotropic under nonuniform flows. We note that since the reptation tube diameter is significantly larger than the Kuhn length, the current version of their model may not be able to resolve interfacial structure and dynamics at interfaces between macro- and microphase-separated domains which are typically on the Kuhn length scale, and are strongly affected by segmental interactions, rather than just by deformation of the reptation tube. To resolve interfacial dynamics in such systems, it is essential to formulate the transport equations for composition and momentum on the Kuhn length scale.

Inspired by Hamiltonian and quantum mechanics, a bracket formalism was developed to describe the time evolution of a set of relevant coarse-grained variables, where a symmetric bracket, representing the dissipative contribution to time evolution, is added to an antisymmetric Poisson bracket, describing conservative time evolution, using the free energy functional (the "Hamiltonian") as a sole generator [38]. The recently proposed general equation for the non-equilibrium reversible-irreversible coupling formalism keeps the Poisson bracket description of conservative dynamics, utilizing the total energy functional as the generator, but uses the total entropy functional as the generator for a Landau-Ginzburg description of dissipative dynamics [39,40].

Mavrantzas and Beris [41,42] used a two-fluid, Hamiltonian model, derived using a bracket formalism, to develop transport and constitutive equations for local *macroscopic* variables in incompressible polymer solutions near a wall, such as the polymer chain concentration, the fluid velocity, and the conformation tensor. The Hamiltonian (extended free

energy) used in the macroscopic equations is specified using a microscopic SCF model for chain conformations, accounting for the simultaneous effect of the solid surface and of the imposed flow field. Their approach accounts for chain stretching and orientation in nonuniform flows by an anisotropic chain propagator, similar to the anisotropic $\lambda^{\alpha}_{\mathbf{a}_k,\mathbf{r}}$ in our DSCF theory. However, the "guiding" equation for their anisotropic chain propagators is not the evolution equation for FENE-P dumbbells representing the second moment of ideal (noninteracting) chains, but rather the evolution equation for an apparent strain tensor for the affine deformation of polymer chains by the flow field. Unlike our equations for the time evolution of composition and momentum, which are formulated on the microscopic, Kuhn length scale, their transport equations for composition and momentum are formulated on a larger, macroscopic scale, and thus are not suitable for resolving interfacial structure and dynamics at typical interfaces between macro- or microphase-separated domains.

Computational advances in recent decades made possible MD simulations of polymer systems [43], based on a numerical integration of Newton's equations of motion for microscopic degrees of freedom. MD simulations provide important insight about the dynamics of unentangled, inhomogeneous polymer fluids at equilibrium [44,45], and under shear [46,47]. However, MD methods suffer from an inherent limitation on the maximum size of the time step used in the numerical integration, which is set by the fastest vibration in the system. This makes MD studies of large, dense, and slowly evolving polymer systems computationally either very costly or out of reach. In addition, fluctuations are enhanced in small systems, thus masking slowly evolving collective trends in MD simulation. The DSCF theory presented here provides a complementary approach that overcomes some of these limitations.

Various mesoscopic methods, based on coarse graining of time and length scales, were developed in an attempt to overcome the limitations of macroscopic and microscopic approaches. Brownian dynamics (BD) methods replace Newtonian microscopic equations of motion, which are used in MD, with Langevin equations of motion for coarse-grained models for chain segments in a fluid, such as the Rouse or elastic dumbbell models [5,6]. BD provides segmental equations of motion at a coarser time scale, accounting for chain stretching, mobility, and stress in response to friction forces exerted by the surrounding fluid (modeled as a continuum) and for random forces (which generate Brownian motion). In the CONNFFESSIT [48] approach for calculation of non-Newtonian flows, viscoelastic stresses determined from such stochastic simulation techniques are coupled to a finite-element formulation of macroscopic continuum transport equations, replacing phenomenological constitutive relations between the stress and the velocity gradients. In such stochastic models, interactions with segments belonging to other chains can be modeled with a self-consistent field [49]. The advantage of BD equations of motion is that they can be simulated even if there is no closure in the corresponding Fokker-Planck equations for the second moments of the normal modes, or of the end-to-end distance. However, this comes at a considerable computational cost.

Dissipative particle dynamics [50,51] (DPD) is a hybrid mesoscopic method that combines elements of BD and lattice-Boltzmann (LB) methods. It is based on an equation of motion for soft spheres, representing either fluid elements or segments in a polymer chain connected by entropic springs [52,53]. As in BD, DPD particles interact pairwise according to a set of short-range forces that include a conservative force, a dissipative force, and a random force. In contrast with BD, and similarly to LB, the surrounding fluid is modeled by discrete mesoscopic particles and not as a continuum. Provided that the dissipative force and the random force satisfy a certain relation, the system has statistical mechanics corresponding to a canonical ensemble with a temperature related to the relative amplitudes of the dissipative and random forces [54]. A repulsive interaction between different types of DPD particles plays a role similar to that of the Flory-Huggins χ parameter in their lattice model of polymer fluids [55]. DPD simulations produce efficient simulations of inhomogeneous polymer fluids at equilibrium. The main problem with DPD dynamics is that the rate of diffusive transport in DPD polymer fluids is of the same order of magnitude as the momentum transport, while in real polymer fluids they differ by many orders of magnitude. The artificially soft repulsive potentials in DPD speed up the diffusive dynamics, but lead to artificially high fluid phase compressibilities, loss of topological constraints between chains, strong fluctuation effects, and often a loss of connection to the chemical details of underlying complex fluids.

While formal projection operator methods extracting dynamic equations for macroscopic variables from a microscopic description of polymer dynamics exist [56,57], the resulting equations that relate microscopic variables to the coarse-grained variables are complicated, limiting the value of this formalism for numerical simulations. A two-fluid model [58,59] allows an efficient generation of Onsager couplings [60] between stress and concentration variables for the Rouse model in the low-frequency limit. More recently, Fredrickson [61] proposed using field theory to obtain the exact thermodynamic forces as functional derivatives of a Hamiltonian corresponding to the "Gaussian thread model" [5] of polymer conformations. He then augmented the time evolution equations of a corresponding two-fluid model containing dissipative coefficients with real noise sources, obtaining a system of coupled complex Langevin equations that can be simulated numerically. Though inherently more accurate than mean field theories, this approach is computationally more demanding. A mean field approximation is recovered by substituting saddle-point values for the fields and neglecting the noise terms in the Langevin equations. Results of actual numerical simulations based on this formalism, or its mean field approximation, are yet to be published.

III. MODEL AND FORMULATION

A. Self-consistent mean field approximation

Consider a fluid composed of two molecular species A and B, each species being a linear homopolymer chain of N^A or N^B freely jointed Kuhn segments, respectively. Let the polymer fluid be confined between two parallel solid walls,

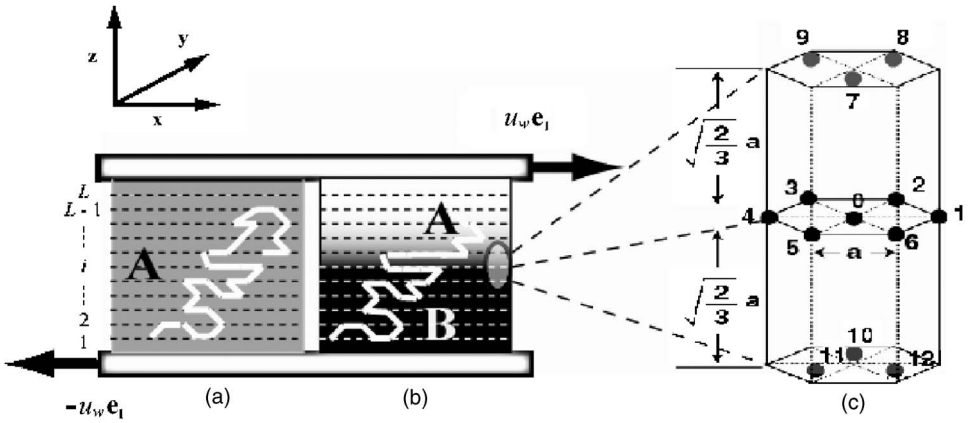

FIG. 1. Inhomogeneous polymer fluids in a channel between two solid walls sheared along the x axis at opposite velocities $\mathbf{u}_w = \pm u_w(1,0,0)$. Some systems are translationally invariant within layers parallel to the walls (dashed lines). Chain conformations shown as biased random walks (solid white lines) in a self-consistent field. (a) A melt of a single species. (b) A phase-separated blend of two species A and B, with the interface between the majority-A and majority-B species parallel to the wall and centered at mid channel. (c) Enlarged view of a site (labeled 0) in a triangular lattice layer i on the fcc lattice, surrounded by all its nearest neighbors, labeled 1–6 in the same layer, 7–9 in the triangular lattice layer $i+1$, and 10–12 in the triangular lattice layer $i-1$.

which are normal to the z axis in an (x,y,z) Cartesian system of coordinates, and are sheared at constant but opposite velocities $(-u_w,0,0)$ and $(u_w,0,0)$, as shown in Fig. 1. Such systems have been studied by MD simulations, using both realistic atomic potentials [45], and coarse-grained bead-spring potentials [44,46,47]. In order to resolve interfacial phenomena, the results of MD simulations are typically analyzed by performing local space and time averages over the MD trajectories ("binning"). The outcome is an evolving set of mean local occupancies and velocities, averaged over a grid of spatial bins. To resolve steep gradients at interfaces, the spatial dimensions of these bins must be comparable to molecular dimensions in the case of simple fluids, and to Kuhn segment dimensions in the case of polymer fluids. The time intervals used for averaging have to be much larger than a single MD time step, but much smaller than the total simulation time. The bin-averaged microscopic evolution arising from MD simulations bears a remarkable resemblance to Eyring's transition-state [1] and Frenkel's kinetic [2] theories of transport in liquids. The bins used in analysis of MD simulations can be associated with molecular or segmental cages moving at a local mean velocity. Small molecules or polymer segments occupying such cages are advected at their local mean velocity, as well as hopping from an occupied cage to an adjacent vacant cage with thermally activated transition rates. Cages may be approximated by lattice unit cells, and the latter identified with the spatial bins used in the binning analysis of MD simulations.

A recent dynamic self-consistent mean field theory for simple fluids [3,4] models the time evolution of the local mean occupancies and velocities on such a lattice of binning grids. It describes the mass and momentum transport on the cage scale, with mass and momentum fluxes including diffusive and viscous contributions modeled as self-consistent stochastic processes with thermally activated hopping rates, as well as convective contributions. It assumes a mean field factorization of joint configurational probabilities into a product of one-body probabilities for molecules interacting with a self-consistent field representing adjacent molecules and walls. The polymer DSCF theory presented here aims at a similar objective for unentangled polymer fluids, a task that is complicated by the need to account for intrachain correlations and for deformation of chain conformations under flow.

Motivated by the discussion above, we start the formulation of our DSCF theory by discretizing the space between a pair of parallel sheared walls into unit cells centered about the sites $\mathbf{r}$ of a face-centered cubic (fcc) lattice [62,63], and forming L triangular lattice layers stacked parallel to the walls, as shown in Fig. 1. Lattice-gas models are widely used to model equilibrium states of simple fluids and are related to the Ising model of ferromagnetism [64]. In lattice-gas models of simple fluids, each unit cell may be occupied by a single molecule. However, flexible linear polymers are approximated by freely jointed chains of Kuhn segments [7]. The simplest lattice-gas model for polymer fluids, the Flory-Huggins (FH) theory [65–67], assumes that each unit cell is occupied by a Kuhn segment.

Let a be the lattice constant of the fcc lattice. We identify a with the larger of the Kuhn lengths of the two homopolymer species. The volume of the Wigner-Seitz unit cell on the fcc lattice is $w=a^3/\sqrt{2}$. Let $\mathbf{e}_1=(1,0,0)$, $\mathbf{e}_2=(0,1,0)$, and $\mathbf{e}_3=(0,0,1)$ be a triad of unit vectors serving as the basis for the (x,y,z) Cartesian system of coordinates. A site $\mathbf{r}=(x,y,z)$ belonging to the fcc lattice has 12 nearest neighbors at $\mathbf{r}+\mathbf{a}_k$, where

$$\mathbf{a}_1 = a(1,0,0) = -\mathbf{a}_4,$$

$$\mathbf{a}_2 = a\left(\frac{1}{2},\frac{\sqrt{3}}{2},0\right) = -\mathbf{a}_5,$$

$$\mathbf{a}_3 = a\left(-\frac{1}{2},\frac{\sqrt{3}}{2},0\right) = -\mathbf{a}_6,$$

$$\mathbf{a}_7 = a\left(0, -\frac{1}{\sqrt{3}}, \sqrt{\frac{2}{3}}\right) = -\mathbf{a}_{10},$$

$$\mathbf{a}_8 = a\left(\frac{1}{2}, \frac{1}{2\sqrt{3}}, \sqrt{\frac{2}{3}}\right) = -\mathbf{a}_{11},$$

$$\mathbf{a}_9 = a\left(-\frac{1}{2}, \frac{1}{2\sqrt{3}}, \sqrt{\frac{2}{3}}\right) = -\mathbf{a}_{12}. \quad (1)$$

The six sites $\{\mathbf{r}+\mathbf{a}_1, \mathbf{r}+\mathbf{a}_2, \mathbf{r}+\mathbf{a}_3, \mathbf{r}+\mathbf{a}_4, \mathbf{r}+\mathbf{a}_5, \mathbf{r}+\mathbf{a}_6\}$ form a nearest-neighbor shell on a triangular lattice within the (x,y) plane at distance z from the origin. The three lattice sites $\{\mathbf{r}+\mathbf{a}_7, \mathbf{r}+\mathbf{a}_8, \mathbf{r}+\mathbf{a}_9\}$, stacked as shown in Fig. 1(c), occupy another triangular lattice on the (x,y) plane at a distance $z+\sqrt{2/3}a$ from the origin. Similarly, the three lattice sites $\{\mathbf{r}+\mathbf{a}_{10}, \mathbf{r}+\mathbf{a}_{11}, \mathbf{r}+\mathbf{a}_{12}\}$, stacked as shown in Fig. 1(c), form another triangular lattice on the plane (x,y) at a distance $z-\sqrt{2/3}a$ from the origin. Our objective is to obtain the time evolution of all relevant dynamic variables defined at the sites of the fcc lattice belonging to L triangular lattice layers parallel to the walls, at $z_i = \sqrt{2/3}ia$ (where $i=1,\ldots,L$). The bottom wall is located in the plane $z=0$, and the sites of the triangular lattice layer adjacent to the bottom wall are located in the plane $z=z_1 \equiv \sqrt{2/3}a$. Similarly, the top wall is in the plane $z=\sqrt{2/3}a(L+1)$, and the sites of the triangular lattice layer adjacent to it are in the plane $z=z_L \equiv \sqrt{2/3}aL$. We assume periodic boundary conditions within the triangular lattice layers.

At any time t, each Wigner-Seitz cell centered at lattice site $\mathbf{r}$ represents a segmental cage advected at an instantaneous mean velocity $\mathbf{u}_\mathbf{r}$. We assume that it is either (a) occupied by a Kuhn segment of type A, in which case the site is assigned an occupancy (pseudospin) variable $\sigma_\mathbf{r}=1$, or (b) occupied by a Kuhn segment of type B, in which case it is assigned an occupancy variable $\sigma_\mathbf{r}=-1$, or (c) vacant, in which case it is assigned an occupancy variable $\sigma_\mathbf{r}=0$. Segments or vacancies occupying this cell have an instantaneous velocity $\mathbf{v}_\mathbf{r}$ which fluctuates about the mean cage velocity $\mathbf{u}_\mathbf{r}$. The microscopic state of the system at time t is specified by the values of the occupancy variables $\sigma_\mathbf{r}$ and the segmental velocities $\mathbf{v}_\mathbf{r}$ assigned to every lattice site $\mathbf{r}$ between the two walls. Denoting the collection of all the sites between the two walls by Ω, the microscopic state is assigned the exact joint probability $P_{ex}(\{\sigma_\mathbf{r}, \mathbf{v}_\mathbf{r}\}_{\mathbf{r}\in\Omega}, t)\Pi_{\mathbf{r}\in\Omega} d\mathbf{v}_\mathbf{r}$, defined at all the lattice sites between the walls. Note that the presence of vacancies makes our DSCF model for polymer fluids *compressible*. In this respect it is different from the original Scheutjens and Fleer lattice SCF theory for equilibrium polymer fluids [68], but is similar to its compressible variants [69–71].

Self-consistent field theories approximate the joint configuration probability for all the constituents in a system with many-body interactions by a product of one-body probabilities for each constituent, interacting solely with a mean external potential field representing interaction with all the other degrees of freedom. In the case of singlet-level SCF lattice-gas models of simple fluids with short-range interactions, and other Ising-like systems, the factorization is over local one-body occupancy probabilities defined at each lattice site. However, the potential at this site is obtained self-consistently by averaging the interaction of a molecule occupying this site with its neighbors using one-body probabilities at adjacent sites, which requires a nonlocal computation. For lattice-gas models of a compressible liquid at equilibrium, the simplest SCF theory is equivalent to the Bragg-Williams theory for the Ising ferromagnet [64,72–74]. An early example of a dynamic mean field theory is Boltzmann's kinetic equation [60] for the time evolution of one-body probability distributions in gases, where products of one-body probabilities approximate pair probabilities. Lattice-Boltzmann methods [75–79] are lattice versions of Boltzmann's kinetic equation. In the continuum limit, they reproduce the description of transport in inhomogeneous fluids by means of partial differential equations (such as the Navier-Stokes, Cahn-Hilliard-Cook [80,81], and time-dependent Landau-Ginzburg [62,82] equations), but are computationally more efficient. The same assumption about factorization of correlations plays a key role in the derivation of kinetic mean field equations from the underlying master equation governing the time evolution of configurational probability in stochastic lattice-gas models [11].

Polymer SCF theory at equilibrium can be formulated by considering the equilibrium statistical mechanics of extended, flexible, interacting chains. However, to gain computational advantage, the statistical mechanics of any system of interacting extended objects can be reduced to statistical mechanics of smaller constituents of the extended objects, with internal interactions, correlations and constraints between the constituents of each extended object. For example, the statistical mechanics of extended molecules is often reduced to the statistical mechanics of constituent atoms or united atoms (as in MD simulations), or of interaction sites (as in the reference interaction site model and its polymer version). We facilitate the nonequilibrium formulation of our DSCF theory for polymer fluids by reducing the statistical mechanics of interacting freely jointed chains to statistical mechanics of Kuhn segments, and regard the latter as basic system constituents.

As in any self-consistent mean field theory formulated on the singlet level, the joint probability for a many-segment system is approximated initially by a product of one-body probabilities for a Kuhn segment of a given type (or a vacancy) to occupy a given site,

$$P_{ex}(\{\sigma_\mathbf{r}, \mathbf{v}_\mathbf{r}\}_{\mathbf{r}\in\Omega}, t)\prod_{\mathbf{r}\in\Omega} d\mathbf{v}_\mathbf{r} = \prod_{\mathbf{r}\in\Omega} P(\sigma_\mathbf{r}, t)Q(\sigma_\mathbf{r}, \mathbf{v}_\mathbf{r}, t)d\mathbf{v}_\mathbf{r}. \quad (2)$$

We refer to $P(\sigma_\mathbf{r}, t)$ as the time-dependent *free segment probability* at site $\mathbf{r}$, since under equilibrium conditions it reduces to the time-independent free segment (monomer) probability originally proposed by Scheutjens and Fleer in their lattice SCF theory for inhomogeneous polymer fluids at thermodynamic equilibrium [68]. $P(\sigma_\mathbf{r}, t)$ is the time-dependent one-body probability for a free segment of type A, or type B, or a vacancy, to be at the lattice site $\mathbf{r}$. The segments occupying this site interact solely with a local potential field, representing interactions of a free segment at this

site with either walls or segments at adjacent sites that belong to freely jointed chains. Note that our model is compressible, since we allow vacancies at lattice sites. Similarly $Q(\sigma_{\mathbf{r}},\mathbf{v}_{\mathbf{r}},t)d\mathbf{v}_{\mathbf{r}}$ is the one-body probability for the velocities $\mathbf{v}_{\mathbf{r}}$ of the respective free segments or vacancies at lattice sites $\mathbf{r}$ to be in a volume element $d\mathbf{v}_{\mathbf{r}}$ in velocity space. A similar factorization approximation was used previously in a mean field study of convective-diffusive model of sheared simple fluids [3,4]. However, in that study, each cage was occupied by a compact atom or molecule, rather than by a Kuhn segment of a polymer chain.

Henceforth we use a local equilibrium approximation for the velocity probability distribution function $Q(\sigma_{\mathbf{r}},\mathbf{v}_{\mathbf{r}},t)$. This means that, locally, it has the same form as the equilibrium Maxwell-Boltzmann distribution of segmental velocities, in the frame of reference of a cage centered at site $\mathbf{r}$ and moving at a mean velocity $\mathbf{u}_{\mathbf{r}}$, and that vacancies are advected at the mean cage velocity $\mathbf{u}_{\mathbf{r}}$, as follows:

$$Q(\sigma_{\mathbf{r}},\mathbf{v}_{\mathbf{r}},t)=\begin{cases}(2\pi m^A k_B T_{\mathbf{r}})^{-3/2}\exp[-m^A(\mathbf{v}_{\mathbf{r}}-\mathbf{u}_{\mathbf{r}})^2/2k_BT_{\mathbf{r}}] & \text{if } \sigma_{\mathbf{r}}=1,\\ (2\pi m^B k_B T_{\mathbf{r}})^{-3/2}\exp[-m^B(\mathbf{v}_{\mathbf{r}}-\mathbf{u}_{\mathbf{r}})^2/2k_BT_{\mathbf{r}}] & \text{if } \sigma_{\mathbf{r}}=-1,\\ \delta(\mathbf{v}_{\mathbf{r}}-\mathbf{u}_{\mathbf{r}}) & \text{if } \sigma_{\mathbf{r}}=0.\end{cases} \quad . \tag{3}$$

Here m^A and m^B are the masses of Kuhn segments of types A and B, respectively, and $T_{\mathbf{r}}$ is the local temperature of the cage centered at site $\mathbf{r}$. The local equilibrium approximation in Eq. (3) neglects the dependence of the velocity probability distribution function on other (second and higher) moments of the velocity. Accounting for this dependence requires better approximations, such as Grad's "thirteen moments" method [10,60]. For the remainder of this paper, we assume that the system is isothermal, so that at all times t, $T_{\mathbf{r}}=T$ for all $\mathbf{r}\in\Omega$, though in the case of simple fluids it has been shown how this assumption can be relaxed to model nonisothermal and Marangoni flows [4]. Since $Q(\sigma_{\mathbf{r}},\mathbf{v}_{\mathbf{r}},t)$ are simple Gaussians or δ functions of $\mathbf{v}_{\mathbf{r}}$, velocity moments such as $\int\mathbf{v}_{\mathbf{r}}^n Q(\sigma_{\mathbf{r}},\mathbf{v}_{\mathbf{r}},t)d\mathbf{v}_{\mathbf{r}}$ are easily evaluated functions of the mean cage velocities $\mathbf{u}_{\mathbf{r}}$ and the temperature T that no longer depend on $\mathbf{v}_{\mathbf{r}}$.

To simplify the form of the equations, we henceforth drop the explicit time dependence of various quantities, and denote $P(\sigma_{\mathbf{r}},t)=P_{\mathbf{r}}^A$ or $P_{\mathbf{r}}^B$ when site $\mathbf{r}$ in layer i is occupied by a segment of species A or B ($\sigma_{\mathbf{r}}=\pm1$), respectively, and $P(\sigma_{\mathbf{r}},t)=1-P_{\mathbf{r}}^A-P_{\mathbf{r}}^B$ when this site is vacant ($\sigma_{\mathbf{r}}=0$). The free segment probabilities $P_{\mathbf{r}}^\alpha$ relate to $\tilde{P}_{\mathbf{r}}^\alpha$, the statistical weights to place a free segment of species α at site $\mathbf{r}$, as

$$P_{\mathbf{r}}^\alpha=\tilde{P}_{\mathbf{r}}^\alpha/(1+\tilde{P}_{\mathbf{r}}^A+\tilde{P}_{\mathbf{r}}^B), \tag{4}$$

and hence

$$\tilde{P}_{\mathbf{r}}^\alpha=P_{\mathbf{r}}^\alpha/(1-P_{\mathbf{r}}^A-P_{\mathbf{r}}^B). \tag{5}$$

According to Eq. (5) a vacancy at a site is always assigned a constant statistical weight of 1 (since vacancies cannot interact with a self-consistent potential), while the statistical weights for a free segment of type A or B to occupy a site can be a non-negative number larger or smaller than 1 (reflecting either an attractive or a repulsive self-consistent potential for free segments of this type occupying the site $\mathbf{r}$, respectively). Equation (4) just states that the free segment probability for a segment of type A or B to occupy site $\mathbf{r}$ equals the statistical weight for this event, normalized by the sum of the statistical weights for all three possible outcomes (a segment of type A, a segment of type B, or a vacancy) at this site. Hence the probabilities for all three possible outcomes at the site sum up to 1, as they should. This assignment of statistical weights for free segments is consistent with the one used by Scheutjens and Fleer in their original derivation of equilibrium SCF lattice theory for incompressible polymer fluids [12].

B. Random walk model for chain conformations and intrachain correlations

Note that Eq. (2) neglects any correlations between clusters of free segments. Thus, in general, the free segment probability $P(\sigma_{\mathbf{r}},t)$ is different from the local segmental volume fraction $\phi_{\mathbf{r}}^\alpha(t)$ of Kuhn segments belonging to freely jointed chains of N^α segments of species α at site $\mathbf{r}$, which reflects the effect of intrachain correlations between segments arising from chain connectivity. The FH theory [65–67] crudely accounts for these correlations by reducing the translational entropy per segment in a system containing chains of N^α connected segments by a factor of $1/N^\alpha$. Thus it assumes that if one segment in a chain is translated, all the other segments belonging to the same chain are translated along with it. However, this is not necessarily true if the chain changes its conformation as it is being translated in an inhomogeneous fluid, due to changing segmental interactions across interfaces. Accounting for such corrections requires a more accurate treatment of the intrachain correlations and of the statistics of chain conformations than in FH theory [83]. This is achieved if, in addition to the many-body interactions, the intrachain correlations between the Kuhn segments are treated self-consistently as well, as both affect the deviations of chain conformations from ideality across interfacial regions. In line with the prevalent terminology of polymer physics, the term "polymer SCF theory" is reserved for such "doubly self-consistent" methods, to distinguish them from FH or related theories, in which only interactions between segments are treated self-consistently.

In SCF theories of inhomogeneous polymer fluids at equilibrium, the local segmental volume fractions $\phi_{\mathbf{r}}^{\alpha}$ at each site are calculated from known values of one-body free segment probabilities $P_{\mathbf{r}}^{\alpha}$ within a sphere of a radius corresponding to the extended length of the freely jointed chain of species α. In the equilibrium lattice SCF approach of Scheutjens and Fleer [68], this is achieved by modeling chain conformations as lattice random walks in a self-consistent potential field. In the continuous version of equilibrium polymer SCF theory [19–22], the random walks are described by a diffusion equation in the self-consistent field, describing the quasi-time-evolution of the probability to find a terminal segment of the chain at a particular position, where the contour length variable plays the role of time.

Consider a homogeneous, three-dimensional melt of identical homopolymer chains at thermodynamic equilibrium, each consisting of N freely jointed Kuhn segments. In such a melt the chains are overlapping (the number of chains in a volume pervaded by each chain is $N^{1/2}$), even if the chains are unentangled (i.e., $N<N_e$, where we adopt a conservative lower bound $N_e \approx 35$ for the mean number of Kuhn segments between entanglements). Beyond the overlap concentration, the repulsive excluded volume interactions between segments belonging to the same chain (which lead to swelling and non-Gaussian scaling for an isolated chain in a good solvent) are screened by the presence of other chains within the pervaded volume of the coil, at length scales exceeding ξ, the correlation length for concentration fluctuations (Flory's theorem [5,7,84]). In a homogeneous melt at thermodynamic equilibrium far from criticality, ξ is close to the Kuhn length a. Both a self-consistent field argument [84] and a perturbation analysis [5] indicate that the second moment of the end-to-end distance $\langle \mathbf{Q}^2 \rangle$ of a chain in a such a melt scales linearly with N, where N is the number of Kuhn segments. Thus the conformations of such chains obey Gaussian statistics similar to that of an ideal (noninteracting) chain. Moreover, it is known [7,84] that a test chain consisting of N_1 Kuhn segments in a melt of chains consisting of N_2 chemically identical Kuhn segments also obeys Gaussian statistics, as long as $N_1<N_2^2$. Such ideal (noninteracting) Gaussian chains are modeled as isotropic lattice random walks [85,86] depositing noninteracting segments at successive lattice sites, with the chain contour length variable s playing the role of time [68]. All possible chain conformations of an ideal chain of N^{α} segments, starting with the first segment being at a given site, are generated recursively with equal statistical weight. At equilibrium, this is done by selecting any of the sites adjacent to the terminus of a chain of s segments with isotropic (equal) single-step displacement (stepping) probability [85,86] $\lambda=1/q$, where q is the lattice coordination number ($q=12$ for the fcc lattice). A segment is then placed at this adjacent site and connected to the terminus of the s-segment chain, producing a conformation of a chain of $s+1$ connected segments. The process is repeated recursively, until a conformation of a chain of N^{α} jointed Kuhn segments is produced. Such a random walk is a Markov chain obeying a master equation [85,86]. The continuum limit of this master equation has the form of a diffusion equation with an isotropic diffusion coefficient, where s plays the role of time. The solution of the diffusion equation subject to a point source initial condition is an isotropic Gaussian with a second moment of the end-to-end distance that is proportional to $N^{\alpha}-1$ [86].

In the lattice SCF theory for equilibrium polymer fluids by Scheutjens and Fleer [68], there are several contributions to the local self-consistent mean potential field for the one-body free segment probability at a particular site $\mathbf{r}$. One contribution is from interactions of a segment at this site with adjacent segments, solvent molecules, and walls, averaged over $\phi_{\mathbf{r}+\mathbf{a}_k}^{\alpha}$, the local *segmental volume fractions* at adjacent sites, rather than over $P_{\mathbf{r}+\mathbf{a}_k}^{\alpha}$, the one-body free segment probabilities. This is needed to account for intrachain correlations: if, instead, the self-consistent field were obtained by averaging over the free segment probabilities $P_{\mathbf{r}}^{\alpha}$, intrachain correlations would have been neglected, resulting in a much worse approximation for interfacial regions of inhomogeneous polymer fluids. Another contribution originates from the effect of intrachain correlations on configurational entropy. If it is assumed that the polymer fluid is incompressible, as in most applications of polymer SCF theory to date, there is an additional contribution to the self consistent field that imposes the incompressibility constraint. A compressible version of lattice SCF theory for polymer fluids at equilibrium has been formulated by Theodorou [69], combining ideas from the Scheutjens and Fleer lattice SCF theory [68] with the equation of state theory of Sanchez and Lacomb [87,88]. Here we adopt a simpler approach to model compressible polymer fluids by introducing a noninteracting monomer solvent species representing vacancies into the Scheutjens-Fleer equilibrium SCF theory [71].

The additional feature of our DSCF theory is that here the two parallel walls are allowed to move at different velocities, driving the fluid out of thermodynamic equilibrium. Thus all quantities of interest may depend on time. Momentum transfer at the walls induces a time-dependent, nonuniform velocity field $\mathbf{u}_{\mathbf{r}}$, representing the mean cage velocities at sites $\mathbf{r}$ [3,4], which is a lattice discretization of the continuous nonuniform velocity field in the real fluid. Such a nonuniform flow field stretches and orients the polymer chains along preferred directions. As a result, the second moment of the chain end-to-end distance becomes anisotropic even in a melt of ideal chains of homogeneous density [6,10,41]. We account for such anisotropic stretching by allowing $\lambda_{\mathbf{a}_k,\mathbf{r}}^{\alpha}$, the stepping probability (from a segment belonging to an ideal chain that is located at site $\mathbf{r}$ to a connected segment at the adjacent site $\mathbf{r}+\mathbf{a}_k$), to be anisotropic and dependent on both position and time. Hence we replace the equilibrium assumption that the stepping probabilities $\{\lambda_{\mathbf{a}_k,\mathbf{r}}^{\alpha}\}$ are isotropic (identical for all k) [68], with a less restrictive reflection symmetry. Explicitly, we assume that at any site $\mathbf{r}$ belonging to the fcc lattice of Fig. 1(c),

$$\lambda_{\mathbf{a}_l,\mathbf{r}}^{\alpha}=\lambda_{\mathbf{a}_k,\mathbf{r}}^{\alpha} \quad \text{if } \mathbf{a}_l=-\mathbf{a}_k. \tag{6}$$

Thus of the 12 stepping probabilities from a site toward its nearest neighbors on the fcc lattice, only six are independent.

At any given time, the statistical weights for conformations of ideal chains generated by such an anisotropic ran-

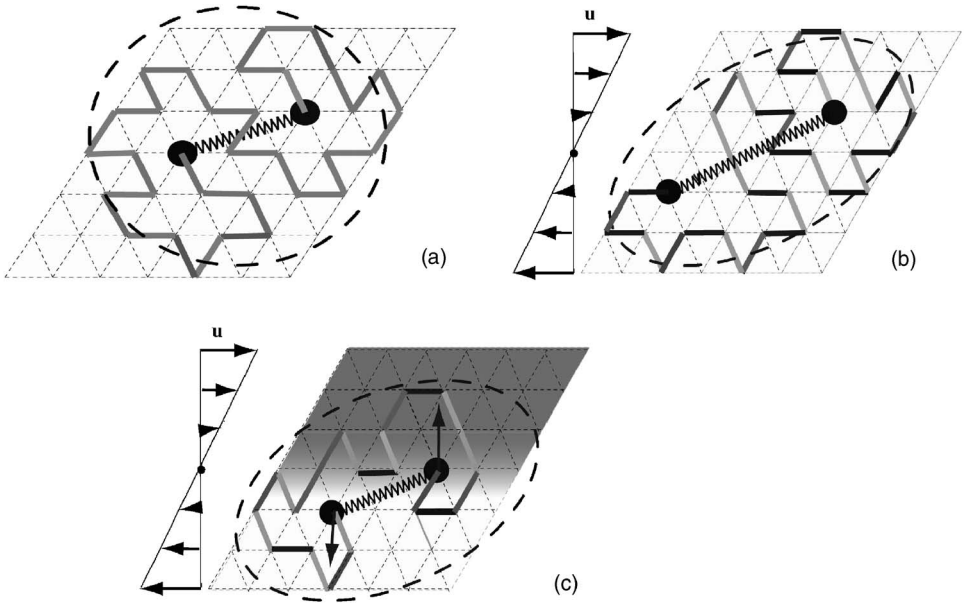

FIG. 2. Random walk and elastic dumbbell representations of chain conformation statistics (for simplicity, a triangular, rather than the fcc lattice, is shown). (a) Chain conformations at equilibrium represented as a lattice random walk (isotropic stepping probabilities denoted by identical bond shading). The isotropic second moment of the end-to-end distance is represented by a sphere. (b) In nonuniform flow, stepping probabilities become anisotropic (denoted by different shading of bonds along different lattice directions). The second moment of the end-to-end distance becomes anisotropic as well (represented by an ellipsoid). (c) Interactions of segments with adjacent segments and with walls in an inhomogeneous polymer fluid are represented by random walk in an external self-consistent field (shaded background).

dom walk [86] procedure will depend on the direction of the steps taken to generate this particular conformation. All possible conformations of chains in a flow field, which interact with other chains or with the walls, are similarly generated by a random walk in a self-consistent mean potential field representing such many-body interactions. The statistical weight to find the terminus of a chain of N^α connected Kuhn segments at any site is found recursively following the algorithm specified by Scheutjens and Fleer [68], but the stepping probabilities for steps toward different nearest neighbors on the fcc lattice are now anisotropic (depend on k), subject to the reflection symmetry constraint Eq. (6). Let $P^\alpha_{\mathbf{r}+\mathbf{a}_k}(s)$ be the statistical weight to find a terminus of a chain of s freely jointed segments of type α at any of the sites $\mathbf{r}+\mathbf{a}_k$ that are adjacent to a given site $\mathbf{r}$. The transition rate to connect an additional segment of type α at site $\mathbf{r}$ to the terminus of an s-segment chain at an adjacent site $\mathbf{r}+\mathbf{a}_k$ is the product of the statistical weight $\tilde{P}^\alpha_{\mathbf{r}}$ for a free segment of type α to be at site $\mathbf{r}$ and an anisotropic stepping probability $\lambda^\alpha_{-\mathbf{a}_k,\mathbf{r}+\mathbf{a}_k}$. The value of $\lambda^\alpha_{\mathbf{a}_k,\mathbf{r}}$ for each bond in the $\mathbf{a}_k$ direction emanating from site $\mathbf{r}$ is represented by the shading of that bond in Fig. 2, and the value of $\tilde{P}^\alpha_{\mathbf{r}}$ at site $\mathbf{r}$ is represented by the background shading. Figure 2 is a schematic representation of a chain conformation generated on a triangular, rather than the fcc lattice, for simplicity reasons. Thus the time-dependent statistical weight $P^\alpha_{\mathbf{r}}(s+1)$ for finding a terminus of an arbitrary α-type subchain of length $s+1$ at the lattice site $\mathbf{r}$ is defined recursively as follows [89]:

$$P^\alpha_{\mathbf{r}}(s+1) = \tilde{P}^\alpha_{\mathbf{r}} \sum_{k=1}^{12} \lambda^\alpha_{-\mathbf{a}_k,\mathbf{r}+\mathbf{a}_k} P^\alpha_{\mathbf{r}+\mathbf{a}_k}(s), \tag{7}$$

with the initial condition $P^\alpha_{\mathbf{r}}(1)=\tilde{P}^\alpha_{\mathbf{r}}$. Equation (7) is a master equation for the evolution of statistical weights $P^\alpha_{\mathbf{r}}(s)$, where the contour length variable s plays the role of time. In the continuous version of polymer SCF theory [19–21] it is replaced by a Chapman-Kolmogorov integro-differential equation [85].

Note that for an ideal, noninteracting chain of type α we have $\tilde{P}^\alpha_{\mathbf{r}}=1$. In this case the background is uniform [shown as a white background in Figs. 2(a) and 2(b)]. If, in addition, the chain and the surrounding fluid are in thermodynamic equilibrium, the values of all the stepping probabilities used in generating the chain are isotropic (independent of bond directions), as represented by identical bond shading for bonds along different directions in Fig. 2(a). The second moment of the distance between the two ends of the chain (denoted by the zigzag line connecting two solid circles) is isotropic [denoted by the dashed circle in Fig. 2(a) corresponding to a sphere on the fcc lattice]. On the other hand, if the fluid has homogeneous composition, but the velocity of the surrounding fluid is nonuniform, stretched and oriented conformations will be assigned higher statistical weights because of higher values of $\lambda^\alpha_{\mathbf{a}_k,\mathbf{r}}$ along preferred bond directions. This is shown by different shading of bonds emanating from each site along different directions $\mathbf{a}_k$. In this case the second moment of the chain end-to-end distance is stretched and anisotropic [denoted by a dashed ellipse in Fig.

2(b), representing an ellipsoid on the fcc lattice]. If, on top of that, the fluid has an inhomogeneous composition, the values of $\tilde{P}_{\mathbf{r}}^{\alpha}$ at different sites will be different [as shown by the nonuniform shading of the background in Fig. 2(c)].

The volume fractions $\phi_{\mathbf{r}}^{\alpha}$ of connected segments of type α occupying a site $\mathbf{r}$ at a given time are calculated from known values of $P_{\mathbf{r}}^{\alpha}(s)$ at that time, as follows [68]:

$$\phi_{\mathbf{r}}^{\alpha} = C_{\alpha} \sum_{s=1}^{N^{\alpha}} \frac{P_{\mathbf{r}}^{\alpha}(s) P_{\mathbf{r}}^{\alpha}(N^{\alpha} - s + 1)}{\tilde{P}_{\mathbf{r}}^{\alpha}}. \tag{8}$$

According to Eq. (8), first the statistical weight for having segment s of an N^{α}-segment chain at site $\mathbf{r}$ is calculated. It is expressed as a product of the statistical weights for two subchains, one of length s and another of length $(N^{\alpha}-s+1)$, to terminate at a common site $\mathbf{r}$, which is then divided by $\tilde{P}_{\mathbf{r}}^{\alpha}$ to compensate for double counting of the statistical weight of placing the terminal segment, which is shared by the two subchains. To get the volume fraction $\phi_{\mathbf{r}}^{\alpha}$ at site $\mathbf{r}$, these statistical weights are then summed over all possible values of s for the common terminal segment along the chain, and normalized. In the continuous version of polymer SCF theory [19–21], the sum over discrete values of s is replaced by an integral over a continuous contour length variable s. The normalization constant is

$$C_{\alpha} = \frac{\bar{\phi}^{\alpha} n_s}{N^{\alpha} \sum_{\mathbf{r}} P_{\mathbf{r}}^{\alpha}(N^{\alpha})}, \tag{9}$$

where n_s is the total number of sites in the system, and $\bar{\phi}^{\alpha}$ is the mean segmental fraction of species α:

$$\bar{\phi}^{\alpha} = \frac{1}{n_s} \sum_{\mathbf{r}} \phi_{\mathbf{r}}^{\alpha}. \tag{10}$$

Note that in a nonreacting, closed system between impermeable walls, $\bar{\phi}^{\alpha}$ is constant. For a two-component A-B blend, we define $\phi_{\mathbf{r}}$, the total segmental volume fraction at site $\mathbf{r}$, and $\bar{\phi}$, the average mean segmental volume fraction, as follows:

$$\phi_{\mathbf{r}} = \phi_{\mathbf{r}}^{A} + \phi_{\mathbf{r}}^{B},$$

$$\bar{\phi} = \bar{\phi}^{A} + \bar{\phi}^{B}. \tag{11}$$

Let m^{α} be the mass of a segment of species α. Then the mass density of species α at site $\mathbf{r}$ is $\rho_{\mathbf{r}}^{\alpha} = m^{\alpha} \phi_{\mathbf{r}}^{\alpha} w^{-1}$. Let

$$\mathbf{g}_{\mathbf{r}}^{\alpha} = \sum_{k=1}^{3} g_{\mathbf{r},k}^{\alpha} \mathbf{e}_k \tag{12}$$

be the momentum density of connected segments belonging to chains of type α at that site; then the local mean velocity of species α is given by

$$\mathbf{u}_{\mathbf{r}}^{\alpha} = \sum_{k=1}^{3} u_{\mathbf{r},k}^{\alpha} \mathbf{e}_k \equiv \left(\frac{w}{m^{\alpha} \phi_{\mathbf{r}}^{\alpha}} \right) \mathbf{g}_{\mathbf{r}}^{\alpha} = \frac{\mathbf{g}_{\mathbf{r}}^{\alpha}}{\rho_{\mathbf{r}}^{\alpha}}. \tag{13}$$

We identify the local mean cage velocity with the mass-averaged mean velocity at the same site, defined by

$$\mathbf{u}_{\mathbf{r}} = \frac{\mathbf{g}_{\mathbf{r}}}{\rho_{\mathbf{r}}}. \tag{14}$$

Here $\mathbf{g}_{\mathbf{r}} = \mathbf{g}_{\mathbf{r}}^{A} + \mathbf{g}_{\mathbf{r}}^{B}$ is the total momentum density and $\rho_{\mathbf{r}} = (m^{A} \phi_{\mathbf{r}}^{A} + m^{B} \phi_{\mathbf{r}}^{B})/w$ is the total mass density at site $\mathbf{r}$.

C. Evolution of anisotropic stepping probabilities

At any moment in time, the modified Scheutjens-Fleer procedure outlined above allows determination of the local segmental volume fractions $\phi_{\mathbf{r}}^{\alpha}$ at all sites $\mathbf{r}$. However, in a system sheared out of thermodynamic equilibrium, this procedure requires as input not only the free segment probabilities $P_{\mathbf{r}}^{\alpha}$, but also the anisotropic stepping probabilities $\lambda_{\mathbf{a}_k,\mathbf{r}}^{\alpha}$, which become functions of position and time. We proceed now to show how to calculate the time evolution of $\lambda_{\mathbf{a}_k,\mathbf{r}}^{\alpha}$.

As stated previously, a homogeneous, one-component homopolymer melt can be considered as a fluid of ideal chains where configurational interactions between segments are negligible. However, the statistical weights for ideal chains are perturbed from their equilibrium values when subjected to flow with nonvanishing velocity gradients [see Eq. (7) and Fig. 2(b)]. Their time evolution should reflect chain stretching and orientation under nonuniform flow, as well as their entropically driven relaxation toward thermodynamic equilibrium. Bead-spring models of such phenomena were constructed for modeling the rheology of unentangled, homogeneous polymer fluids [5,6,8,9]. A homopolymer chain consisting of N^{α} identical, freely jointed Kuhn segments in an unentangled homogeneous melt, can be represented by the Rouse model [90], consisting of N^{α} beads connected by entropic springs, subject to friction and random forces exerted by the surrounding fluid.

Here we adopt an even simpler elastic dumbbell [6] model for the time evolution of the second moment $\mathbf{S}_{\mathbf{r}}^{\alpha} = \langle \mathbf{Q}_{\mathbf{r}}^{\alpha} \mathbf{Q}_{\mathbf{r}}^{\alpha} \rangle$ of the end-to-end distance $\mathbf{Q}_{\mathbf{r}}^{\alpha}$ of an ideal (noninteracting) chain in a homogeneous fluid undergoing nonuniform flow (in Fig. 2, solid circles represent the two beads and the zigzag line represents the elastic spring). A Hookean dumbbell consisting of two beads connected by a linear spring [91,92] has unbounded end-to-end distance, which is not realistic. Here we use the so-called FENE-P dumbbell model — a finitely extensible, nonlinear elastic spring in the Peterlin approximation [13–18], where the nonlinear spring force is *preaveraged* over the probability distribution of end-to-end distances. Thus in our DSCF theory, the effect of the local velocity gradient $\nabla \mathbf{u}_{\mathbf{r}}$ on conformation statistics of an ideal (noninteracting) test chain of N^{α} Kuhn segments placed in homogeneous fluid with its center of mass being positioned at $\mathbf{r}$, is computed using the FENE-P dumbbell model for the time evolution of $\mathbf{S}_{\mathbf{r}}^{\alpha}$, which is a function of $\nabla \mathbf{u}_{\mathbf{r}}$ and of an entropically driven relaxation time.

Let $\mathbf{Q}_{\mathbf{r}}^{\alpha}$ be the end-to-end distance of an ideal (noninteracting) test chain of N^{α} freely jointed Kuhn segments joined

by $N^\alpha-1$ rigid links, of length a each, with its center of mass positioned at $\mathbf{r}$, where the mass-averaged fluid velocity and its gradient are $\mathbf{u}_\mathbf{r}$ and $\nabla\mathbf{u}_\mathbf{r}$. We use a FENE-P dumbbell model for the time evolution of the probability distribution of $\mathbf{Q}_\mathbf{r}^\alpha$ and its second moment. In this model, $\mathbf{Q}_\mathbf{r}^\alpha$ is the distance between the two dumbbell beads (representing the two ends of the freely jointed chain of N^α Kuhn segments), connected by an entropic spring with a spring constant given by $3k_BT\{(N^\alpha-1)\tilde{a}_\alpha^2[1-\langle(\mathbf{Q}_\mathbf{r}^\alpha)^2/Q_0^2\rangle]\}^{-1}$. Here Q_0 is the maximum extension of the spring [13–18], and $\tilde{a}_\alpha=c_\alpha a$ is a length proportional to the Kuhn length. We approximate the probability for such a test chain to have an end-to-end distance between $\mathbf{Q}_\mathbf{r}^\alpha$ in a volume element $d^3\mathbf{Q}_\mathbf{r}^\alpha$ by $\psi_\mathbf{r}^\alpha(\mathbf{Q}_\mathbf{r}^\alpha)d^3\mathbf{Q}_\mathbf{r}^\alpha$, where $\psi_\mathbf{r}^\alpha(\mathbf{Q}_\mathbf{r}^\alpha)$ is the probability density for an ideal (noninteracting) FENE-P test dumbbell to have the same end-to-end distance when its center of mass is positioned at $\mathbf{r}$, where the mass-averaged fluid velocity is $\mathbf{u}_\mathbf{r}$. The time evolution of the probability distribution $\psi_\mathbf{r}^\alpha(\mathbf{Q}_\mathbf{r}^\alpha)$ is described by a Smoluchowski equation [6,18]. In continuous space, the time evolution of the second-rank symmetric tensor $\mathbf{S}_\mathbf{r}^\alpha=\langle\mathbf{Q}_\mathbf{r}^\alpha\mathbf{Q}_\mathbf{r}^\alpha\rangle$ is derived by evaluating the second moment of each term in the Smoluchowski equation, resulting in the following equation [6,18]:

$$\overset{\nabla}{\mathbf{S}}{}_\mathbf{r}^\alpha=-\frac{1}{\tau_{db,\mathbf{r}}^\alpha}\left[\frac{\mathbf{S}_\mathbf{r}^\alpha}{1-[3/(N^\alpha-1)\tilde{a}_\alpha^2b^\alpha]\mathrm{Tr}\mathbf{S}_\mathbf{r}^\alpha}-\frac{(N^\alpha-1)\tilde{a}_\alpha^2}{3}\boldsymbol{\delta}\right], \tag{15}$$

where $\overset{\nabla}{\mathbf{S}}{}_\mathbf{r}^\alpha=D\mathbf{S}_\mathbf{r}^\alpha/Dt-(\nabla\mathbf{u}_\mathbf{r})^T\cdot\mathbf{S}_\mathbf{r}^\alpha-\mathbf{S}_\mathbf{r}^\alpha\cdot(\nabla\mathbf{u}_\mathbf{r})$ is the upper-convected time derivative of $\mathbf{S}_\mathbf{r}^\alpha$ and $D\mathbf{S}_\mathbf{r}^\alpha/Dt=\partial\mathbf{S}_\mathbf{r}^\alpha/\partial t+\mathbf{u}_\mathbf{r}\cdot\nabla\mathbf{S}_\mathbf{r}^\alpha$ is its material derivative. The local mass-averaged velocity $\mathbf{u}_\mathbf{r}$ is calculated from Eq. (14) using Eqs. (4)–(11), and the values of the free segment probabilities $P_\mathbf{r}^\alpha$ and the momentum densities $\mathbf{g}_\mathbf{r}^\alpha$ resulting from the transport equations (28) and (54), as described in Sec. III D. Here the dimensionless finite extensibility parameter [18]

$$b^\alpha=\frac{3\tau_{Q,\mathbf{r}}^\alpha(N^\alpha)}{\tau_{db,\mathbf{r}}^\alpha(N^\alpha)}=3(N^\alpha-1) \tag{16}$$

is thrice the ratio between the relaxation time

$$\tau_{Q,\mathbf{r}}^\alpha(N^\alpha)=\frac{N^\alpha(N^\alpha-1)^2\tilde{a}_\alpha^2\zeta_\mathbf{r}^\alpha}{24k_BT} \tag{17}$$

of a rigid dumbbell of extension $(N^\alpha-1)\tilde{a}_\alpha$, and the relaxation time

$$\tau_{db,\mathbf{r}}^\alpha=\frac{N^\alpha(N^\alpha-1)\tilde{a}_\alpha^2\zeta_\mathbf{r}^\alpha}{24k_BT} \tag{18}$$

of a Hookean dumbbell with spring constant $3k_BT/[(N^\alpha-1)\tilde{a}_\alpha^2]$. Note that $\tau_{db,\mathbf{r}}^\alpha$ is proportional to a local segmental friction coefficient $\zeta_\mathbf{r}^\alpha$. In the limit $b^\alpha\to\infty$, Eq. (15) becomes the evolution equation for the second moment of the end-to-end distance of such a Hookean dumbbell.

At thermodynamic equilibrium, the second moment of the end-to-end distance a chain consisting of N^α Kuhn segments, joined together by $N^\alpha-1$ freely jointed links, each of length a, is a diagonal second-rank tensor with isotropic diagonal components having common value $(N^\alpha-1)a^2/3$. On the other hand, the equilibrium solution of Eq. (15) governing the evolution of $\mathbf{S}_\mathbf{r}^\alpha$ for the FENE-P dumbbell model with the spring constant $3k_BT\{(N^\alpha-1)\tilde{a}_\alpha^2[1-\langle(\mathbf{Q}_\mathbf{r}^\alpha)^2/Q_0^2\rangle]\}^{-1}$ yields

$$S_{\mathbf{r},xx}^\alpha=S_{\mathbf{r},yy}^\alpha=S_{\mathbf{r},zz}^\alpha=\left(\frac{b^\alpha}{b^\alpha+3}\right)\frac{(N^\alpha-1)\tilde{a}_\alpha^2}{3},$$
$$S_{\mathbf{r},xy}^\alpha=S_{\mathbf{r},yz}^\alpha=S_{\mathbf{r},xz}^\alpha=0, \tag{19}$$

where $\tilde{a}_\alpha=c_\alpha a$. Thus Eq. (19) recovers the equilibrium value of $\mathbf{S}_\mathbf{r}^\alpha$ expected for a freely jointed chain of N^α Kuhn segments only if the FENE-P spring constant is tuned so that the relation $c_\alpha=\sqrt{(b^\alpha+3)/b^\alpha}$ is satisfied.

We proceed now to establish a relation between the values of $\mathbf{S}_\mathbf{r}^\alpha$ and the values of $\lambda_{\mathbf{a}_k,\mathbf{r}}^\alpha$ at any given moment in time. We know that in the FENE-P dumbbell model, the probability density $\psi_\mathbf{r}^\alpha(\mathbf{Q}_\mathbf{r}^\alpha)$ for $\mathbf{Q}_\mathbf{r}^\alpha$, which is the solution of the appropriate Smoluchowski equation, has the form [6,18]

$$\psi_\mathbf{r}^\alpha(\mathbf{Q}_\mathbf{r}^\alpha)=\frac{\exp\left[-\frac{1}{2}(\mathbf{S}_\mathbf{r}^\alpha)^{-1}:\mathbf{Q}_\mathbf{r}^\alpha\mathbf{Q}_\mathbf{r}^\alpha\right]}{\sqrt{(2\pi)^3\det(\mathbf{S}_\mathbf{r}^\alpha)}}. \tag{20}$$

In the equation above, $\mathbf{S}_\mathbf{r}^\alpha$ at any particular time is obtained as a solution of Eq. (15) for a FENE-P dumbbell with its center of mass at position $\mathbf{r}$, which requires the history of $\mathbf{u}_\mathbf{r}$ and $\nabla\mathbf{u}_\mathbf{r}$ at prior times as an input. $\mathbf{S}_\mathbf{r}^\alpha$ approximates the second moment of the end-to-end distance of a freely jointed chain of Kuhn segments with its center of mass at position $\mathbf{r}$. One can then ask what would be the simplest model of the same ideal, freely jointed chain of Kuhn segments as a random walk on the fcc lattice at zero external potential that reproduces the same distribution of end-to-end distances as Eq. (20). This case corresponds to setting $\tilde{P}_\mathbf{r}^\alpha=1$ for all $\mathbf{r}$ in Eq. (7), which thus assumes the form

$$P_\mathbf{r}^\alpha(s+1)=\sum_{k=1}^{12}\lambda_{-\mathbf{a}_k,\mathbf{r}+\mathbf{a}_k}^\alpha P_{\mathbf{r}+\mathbf{a}_k}^\alpha(s), \tag{21}$$

where $P_\mathbf{r}^\alpha(1)=1$. To obtain the simplest random walk model reproducing the properties of the FENE-P dumbbell model under flow, we assume that $\lambda_{\mathbf{a}_k,\mathbf{r}'}^\alpha=\lambda_{\mathbf{a}_k,\mathbf{r}}^\alpha$ for segments at sites $\mathbf{r}'$ belonging to the same freely jointed chain of Kuhn segments with its center of mass at position $\mathbf{r}$. Subtracting $P_\mathbf{r}^\alpha(s)$ from both sides of this equation, and using $\Sigma_{k=1}^{12}\lambda_{\mathbf{a}_k,\mathbf{r}}^\alpha=1$, we then get

$$P_\mathbf{r}^\alpha(s+1)-P_\mathbf{r}^\alpha(s)=\sum_{k=1}^{12}[\lambda_{-\mathbf{a}_k,\mathbf{r}+\mathbf{a}_k}^\alpha P_{\mathbf{r}+\mathbf{a}_k}^\alpha(s)-\lambda_{\mathbf{a}_k,\mathbf{r}}^\alpha P_\mathbf{r}^\alpha(s)]. \tag{22}$$

This is a master equation generating statistical weights for finding the terminus of an ideal (noninteracting) chain at $\mathbf{r}$ in a homogeneous fluid undergoing nonuniform flow characterized by a mass-averaged velocity gradient $\nabla\mathbf{u}_\mathbf{r}$, modeled as a biased random walk on a fcc lattice. Expanding Eq. (22) in a Taylor series to first order in s and to second order in space, and neglecting spatial variation of $\lambda_{\mathbf{a}_k,\mathbf{r}}^\alpha$ over the length scale

of the chain end-to-end vector, we see that $P_{\mathbf{r}}^{\alpha}(s)$ satisfies a diffusion equation

$$\frac{\partial P_{\mathbf{r}}^{\alpha}(s)}{\partial s} = \mathbf{\Lambda}_{\mathbf{r}}^{\alpha}:\boldsymbol{\nabla}\boldsymbol{\nabla} P_{\mathbf{r}}^{\alpha}(s), \tag{23}$$

where the contour length variable s plays the role of time, and the initial condition is $P_{\mathbf{r}}^{\alpha}(0)=\delta(\mathbf{r})$. Using the symmetry $\lambda_{-\mathbf{a}_k,\mathbf{r}}^{\alpha}=\lambda_{\mathbf{a}_k,\mathbf{r}}^{\alpha}$ at each site and collecting terms from the Taylor expansion, we get

$$\Lambda_{xx,\mathbf{r}}^{\alpha} = a^2\left[\lambda_{\mathbf{a}_1,\mathbf{r}}^{\alpha} + \frac{1}{4}(\lambda_{\mathbf{a}_2,\mathbf{r}}^{\alpha} + \lambda_{\mathbf{a}_3,\mathbf{r}}^{\alpha} + \lambda_{\mathbf{a}_8,\mathbf{r}}^{\alpha} + \lambda_{\mathbf{a}_9,\mathbf{r}}^{\alpha})\right],$$

$$\Lambda_{yy,\mathbf{r}}^{\alpha} = a^2\left[\frac{3}{4}(\lambda_{\mathbf{a}_2,\mathbf{r}}^{\alpha} + \lambda_{\mathbf{a}_3,\mathbf{r}}^{\alpha}) + \frac{1}{3}\lambda_{\mathbf{a}_7,\mathbf{r}}^{\alpha} + \frac{1}{12}(\lambda_{\mathbf{a}_8,\mathbf{r}}^{\alpha} + \lambda_{\mathbf{a}_9,\mathbf{r}}^{\alpha})\right],$$

$$\Lambda_{zz,\mathbf{r}}^{\alpha} = a^2\left[\frac{2}{3}(\lambda_{\mathbf{a}_7,\mathbf{r}}^{\alpha} + \lambda_{\mathbf{a}_8,\mathbf{r}}^{\alpha} + \lambda_{\mathbf{a}_9,\mathbf{r}}^{\alpha})\right],$$

$$\Lambda_{xy,\mathbf{r}}^{\alpha} = a^2\left[\frac{\sqrt{3}}{4}(\lambda_{\mathbf{a}_2,\mathbf{r}}^{\alpha} - \lambda_{\mathbf{a}_3,\mathbf{r}}^{\alpha}) + \frac{1}{4\sqrt{3}}(\lambda_{\mathbf{a}_8,\mathbf{r}}^{\alpha} - \lambda_{\mathbf{a}_9,\mathbf{r}}^{\alpha})\right],$$

$$\Lambda_{yz,\mathbf{r}}^{\alpha} = a^2\left[\frac{\sqrt{2}}{6}(\lambda_{\mathbf{a}_8,\mathbf{r}}^{\alpha} + \lambda_{\mathbf{a}_9,\mathbf{r}}^{\alpha} - 2\lambda_{\mathbf{a}_7,\mathbf{r}}^{\alpha})\right],$$

$$\Lambda_{xz,\mathbf{r}}^{\alpha} = a^2\left[\frac{1}{\sqrt{6}}(\lambda_{\mathbf{a}_8,\mathbf{r}}^{\alpha} - \lambda_{\mathbf{a}_9,\mathbf{r}}^{\alpha})\right]. \tag{24}$$

The solution of Eq. (23) for $P_{\mathbf{r}+\mathbf{Q}_{\mathbf{r}}^{\alpha}}^{\alpha}(N^{\alpha}-1)$ with the initial condition $P_{\mathbf{r}}^{\alpha}(0)=\delta(\mathbf{r})$ is

$$P_{\mathbf{r}+\mathbf{Q}_{\mathbf{r}}^{\alpha}}^{\alpha}(N^{\alpha}-1) = \frac{\exp\left\{-\frac{1}{2}[2(N^{\alpha}-1)\mathbf{\Lambda}_{\mathbf{r}}^{\alpha}]^{-1}:\mathbf{Q}_{\mathbf{r}}^{\alpha}\mathbf{Q}_{\mathbf{r}}^{\alpha}\right\}}{\sqrt{(2\pi)^3\det[2(N^{\alpha}-1)\mathbf{\Lambda}_{\mathbf{r}}^{\alpha}]}}. \tag{25}$$

By comparing Eq. (25) with Eq. (20), we get a system of six linear equations,

$$\mathbf{S}_{\mathbf{r}}^{\alpha} = 2(N^{\alpha}-1)\mathbf{\Lambda}_{\mathbf{r}}^{\alpha}. \tag{26}$$

Solving Eq. (24) for the six independent stepping probabilities at each site, we get

$$\lambda_{\mathbf{a}_1,\mathbf{r}}^{\alpha} = \frac{1}{(N^{\alpha}-1)a^2}\left(\frac{1}{2}S_{xx,\mathbf{r}}^{\alpha} - \frac{1}{6}S_{yy,\mathbf{r}}^{\alpha} - \frac{1}{12}S_{zz,\mathbf{r}}^{\alpha} - \frac{1}{3\sqrt{2}}S_{yz,\mathbf{r}}^{\alpha}\right),$$

$$\lambda_{\mathbf{a}_2,\mathbf{r}}^{\alpha} = \frac{1}{(N^{\alpha}-1)a^2}\left(\frac{1}{3}S_{yy,\mathbf{r}}^{\alpha} - \frac{1}{12}S_{zz,\mathbf{r}}^{\alpha} + \frac{1}{\sqrt{3}}S_{xy,\mathbf{r}}^{\alpha} + \frac{1}{6\sqrt{2}}S_{yz,\mathbf{r}}^{\alpha} - \frac{1}{2\sqrt{6}}S_{xz,\mathbf{r}}^{\alpha}\right),$$

$$\lambda_{\mathbf{a}_3,\mathbf{r}}^{\alpha} = \frac{1}{(N^{\alpha}-1)a^2}\left(\frac{1}{3}S_{yy,\mathbf{r}}^{\alpha} - \frac{1}{12}S_{zz,\mathbf{r}}^{\alpha} - \frac{1}{\sqrt{3}}S_{xy,\mathbf{r}}^{\alpha} + \frac{1}{6\sqrt{2}}S_{yz,\mathbf{r}}^{\alpha} + \frac{1}{2\sqrt{6}}S_{xz,\mathbf{r}}^{\alpha}\right),$$

$$\lambda_{\mathbf{a}_7,\mathbf{r}}^{\alpha} = \frac{1}{(N^{\alpha}-1)a^2}\left(\frac{1}{4}S_{zz,\mathbf{r}}^{\alpha} - \frac{1}{\sqrt{2}}S_{yz,\mathbf{r}}^{\alpha}\right),$$

$$\lambda_{\mathbf{a}_8,\mathbf{r}}^{\alpha} = \frac{1}{(N^{\alpha}-1)a^2}\left(\frac{1}{4}S_{zz,\mathbf{r}}^{\alpha} + \frac{1}{2\sqrt{2}}S_{yz,\mathbf{r}}^{\alpha} + \frac{\sqrt{6}}{4}S_{xz,\mathbf{r}}^{\alpha}\right),$$

$$\lambda_{\mathbf{a}_9,\mathbf{r}}^{\alpha} = \frac{1}{(N^{\alpha}-1)a^2}\left(\frac{1}{4}S_{zz,\mathbf{r}}^{\alpha} + \frac{1}{2\sqrt{2}}S_{yz,\mathbf{r}}^{\alpha} - \frac{\sqrt{6}}{4}S_{xz,\mathbf{r}}^{\alpha}\right). \tag{27}$$

The last equation expresses, for any particular time, each of the six independent stepping probabilities $\lambda_{\mathbf{a}_k,\mathbf{r}}^{\alpha}$ from site $\mathbf{r}$ as a linear combination [normalized by $(N^{\alpha}-1)a^2$] of the six independent components of the symmetric, second-rank tensor $\mathbf{S}_{\mathbf{r}}^{\alpha}$ of the second moment of the end-to-end distance of a FENE-P dumbbell, with its center of mass at position $\mathbf{r}$, given the history of $\mathbf{u}_{\mathbf{r}}$ and $\boldsymbol{\nabla}\mathbf{u}_{\mathbf{r}}$ at prior times. These stepping probabilities $\lambda_{\mathbf{a}_k,\mathbf{r}}^{\alpha}$ can then be used in Eq. (7) to generate the statistical weights for the terminal probabilities of interacting chains of jointed Kuhn segments at site $\mathbf{r}$, modeled as random walks in an inhomogeneous self-consistent potential field representing the interactions. Substituting Eq. (19) [the equilibrium solution of Eq. (15)] into Eq. (27), we recover the equilibrium SCF values $\lambda_{\mathbf{a}_k,\mathbf{r}}^{\alpha}=\frac{1}{12}$.

In a sense, the FENE-P dumbbell serves as a probe for measuring the extent of local stretching and orientation caused by nonuniform flow. Although the length scale of the square roots of the eigenvalues of $\mathbf{S}_{\mathbf{r}}^{\alpha}$ is of order $(N^{\alpha}-1)^{1/2}a$, the components of $\mathbf{S}_{\mathbf{r}}^{\alpha}$ vary on the same length scale as $\mathbf{u}_{\mathbf{r}}$ and $\boldsymbol{\nabla}\mathbf{u}_{\mathbf{r}}$. It will be shown in the next subsection that $\mathbf{u}_{\mathbf{r}}$ and $\boldsymbol{\nabla}\mathbf{u}_{\mathbf{r}}$, as well as $P_{\mathbf{r}}^{\alpha}$ and $\phi_{\mathbf{r}}^{\alpha}$, vary on the Kuhn length scale a. Thus our DSCF model resolves the variation of stepping probabilities $\lambda_{\mathbf{a}_k,\mathbf{r}}^{\alpha}$ on the Kuhn length scale a. This is analogous to using a magnetic compass with a needle of finite length, as a probe to map fine spatial variations in the orientation of a magnetic field by centering the compass at grid points with a smaller spacing than the length of the needle.

D. Self-consistent mean field transport theory

1. Main ideas and relation to existing methodologies

At any given time, local composition and kinematics in our inhomogeneous polymer fluid is described by the values of $\phi_{\mathbf{r}}^{\alpha}$ and $\mathbf{u}_{\mathbf{r}}^{\alpha}$, and local rheology by the relation between the local deviatoric stress and the rate of strain $\boldsymbol{\nabla}\mathbf{u}_{\mathbf{r}}$. The segmental volume fractions $\phi_{\mathbf{r}}^{\alpha}$ are determined from Eq. (8), using input from Eqs. (5), (7), (9), and (10), provided that $P_{\mathbf{r}}^{\alpha}$ and $\lambda_{\mathbf{a}_k,\mathbf{r}}^{\alpha}$ are known. The latter are related by Eq. (27) to the second moment $\mathbf{S}_{\mathbf{r}}^{\alpha}$ of the end-to-end distance of FENE-P dumbbells under nonuniform flow in a homogeneous fluid. Their time evolution is described by Eq. (15), which depends on the mass-averaged velocity $\mathbf{u}_{\mathbf{r}}$ that is, in turn, a function of segmental momentum densities $\mathbf{g}_{\mathbf{r}}^{\alpha}$, given by Eq. (13). Hence, if we know how to calculate the time evolution of $P_{\mathbf{r}}^{\alpha}$ and $\mathbf{g}_{\mathbf{r}}^{\alpha}$ at each site $\mathbf{r}$ on the fcc lattice, we can obtain $\mathbf{S}_{\mathbf{r}}^{\alpha}$, $\lambda_{\mathbf{a}_k,\mathbf{r}}^{\alpha}$, and $\phi_{\mathbf{r}}^{\alpha}$ as well. Thus, in order to get a self-consistent,

closed system of equations, it is necessary to augment the equations derived above with a set of time evolution equations for $P_{\mathbf{r}}^{\alpha}$ and $\mathbf{g}_{\mathbf{r}}^{\alpha}$.

Our evolution equations for $P_{\mathbf{r}}^{\alpha}$ and $\mathbf{g}_{\mathbf{r}}^{\alpha}$ have the form of transport equations obtained by balancing fluxes of $P_{\mathbf{r}}^{\alpha}$ or $\mathbf{g}_{\mathbf{r}}^{\alpha}$ across the boundaries of a control volume of *segmental* dimensions, which is a unit cell of our fcc lattice. The flux expressions are derived using a mean field approximation of the joint probabilities by products of one-body probabilities and segmental volume fractions. This resembles derivation of transport equations arising from both the continuous [60] and lattice [75–79] versions of Boltzmann's kinetic theory for simple fluids [60], where the collision cross section on a molecular scale determines the control volume. It bears even greater resemblance to the diffusive transport equations derived in kinetic mean field theories [11] for stochastic lattice gases [93–95] from a microscopic master equation. Diffusive dynamics in stochastic lattice gases and other Ising-like systems are modeled microscopically as thermally activated, stochastic pair exchange events between adjacent sites [93,94]. The exchange occurs only if the adjacent sites are occupied by a molecule and a vacancy in a lattice gas model, or by opposite pseudospins in an Ising system. The activated pair exchange events occur with certain transition rates depending on the change in the nonequilibrium free energy caused by the pair exchange, in dimensionless units set by the temperature. To assure convergence to thermodynamic equilibrium, the transition rates have to satisfy a local detailed balance condition. The time scale for the transition rate is set by the appropriate diffusion constant. The time evolution of the system's configurational probability is a Markov process governed by a master equation [93].

The complexity of the problem precludes an analytic solution to the master equation, except for very simple limiting cases. Such Markov processes can be simulated directly using Monte Carlo methods [96], which do not neglect many-body correlations, but have strong local fluctuations that may blur the connection to mesoscopic descriptions, such as the Cahn-Hilliard-Cook [81,97], time-dependent Landau-Ginzburg [62,82], and phase-field models [98,99]. This is avoided by the kinetic mean field theories [11] that were developed for stochastic lattice-gas models [100,101]. Similarly to equilibrium mean field theories, kinetic mean field theories approximate the configurational joint probability for system constituents by a product of one-body probabilities for each microscopic constituent, interacting solely with an external potential field. The interaction of a constituent with its conjugate field is expressed as a mean configurational energy of interaction with all the other system constituents. However, in *kinetic* mean field theories both the mean potential fields and the one-body probability distributions are time dependent. The time evolution of the local one-body probabilities and of the self-consistent fields is obtained by balancing fluxes of one-body probabilities about a control volume on molecular length scale. The resulting transport equations are formulated on this scale. The factorization of joint probabilities into a product of one-body probabilities suppresses correlations and fluctuations in these models, making them akin to mesoscopic, deterministic transport equations, such as Cahn-Hilliard-Cook [81,97] and time-dependent Landau-Ginzburg [62,82] equations, typically described by high-order, nonlinear PDEs. They are very different from classical macroscopic equations, such as the diffusion or Fokker-Plank equations, which are typically linear, second-order PDEs with Gaussian solutions describing fluctuations about a deterministically evolving mean. The latter can be formally obtained as a low-order truncation of the so-called Ω expansion of the master equation in powers of $\Omega^{(1-n)/2}$ developed by van Kampen [85], where Ω is associated with the number of microscopic constituents in a minimal control volume. Low-order truncation of the Ω expansion is justified only for large Ω, and, as noted by van Kampen [85], keeping successively higher-order terms in the Ω expansion gives rise to higher-order derivatives and nonlinear coupling in the resulting PDEs for the continuous probability density, which are responsible for the deviation of fluctuations from a Gaussian distribution. Indeed, when binning averages are performed on trajectories of MD simulations using bins with spatial dimensions approaching the dimensions of a single constituent, the resulting averages typically exhibit strong fluctuations which cannot be described as small Gaussian fluctuations about a deterministically evolving mean.

A dynamic SCF lattice gas model for simple fluids has been derived by Khan and Shnidman [3,4], and used for molecular-scale computational modeling of interfacial and wetting flows. Their model includes convective contributions to one-body probability fluxes due to cage advection, as well as a diffusive contribution to the one-body probability fluxes arising from activated hopping between cages as described above. Momentum fluxes similarly include a convective contribution due to cage advection, a viscous contribution from momentum transferred by activated hops, as well as a term representing friction forces generated by net cage velocities arising from biased hopping across bonds. This dynamic SCF model for simple fluids has been used successfully to study both isothermal and nonisothermal interfacial and wetting dynamics in one-, two-, and three-component compressible simple fluids. Truncated Taylor expansions of the evolution equations of this DSCF lattice model lead to continuous evolution equations similar to those of Model H [62,82], a time-dependent Landau-Ginzburg model coupling convective and diffusive transport of local mean species densities with convective and viscous transport of momentum.

Note that the PDEs describing the continuous phenomenological models above indeed involve higher- (fourth-) order derivative terms and nonlinearities which are crucial for modeling interfacial dynamics. Our transport equations have instead the form of a system of nonlinear ODEs. Using truncated Taylor expansions, they can be approximated by a system of nonlinear, higher-order PDEs similar in form to the continuous, deterministic transport models formulated phenomenologically on the mesoscopic scale. However, truncation of the Ω expansions at higher orders leads to unphysical behavior, such as violation of the positivity of the probability, and of its approach to a steady state [85].

A central objective of our polymer DSCF theory is to extend the approach above to unentangled polymer fluids. This requires accounting for intrachain correlations and for deformation of chain conformations under flow.

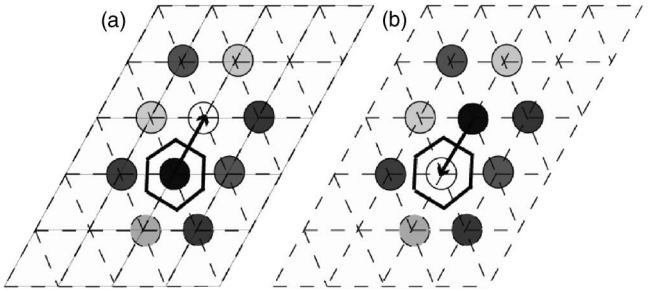

FIG. 3. Hopping contributions to the diffusive and viscous center-of-mass fluxes transporting mass and momentum. (a) A segment (denoted by the black solid circle) hopping out of an occupied site enclosed by a Wigner-Seitz control volume), into a vacant site (denoted by the white circle). The different shading of circles at the surrounding sites denotes different mean segmental volume fractions used to calculate the inhomogeneous self-consistent field at the central site. (b) A reverse hop by a segment at the neighboring site into the vacant site enclosed by the same control volume.

2. Time evolution of free segment probabilities

The balance of fluxes of one-body probabilities $P_{\mathbf{r}}^{\alpha}$ of species α across a unit cell centered at site $\mathbf{r}$ leads to the following time evolution equation for the free segment probability density of species α within the control volume of a unit cell:

$$\frac{dP_{\mathbf{r}}^{\alpha}}{dt} = -\nabla \cdot (P_{\mathbf{r}}^{\alpha}\mathbf{u}_{\mathbf{r}}) - \sum_{k=1}^{12} \frac{\mathbf{j}_{\mathbf{r},\mathbf{r}+\mathbf{a}_k}^{\alpha}}{a}. \tag{28}$$

The first term on the right-hand side (RHS) of Eq. (28) is the divergence of convective fluxes of free segment probabilities. In our computations we use a second-order centered difference approximation for the fcc lattice, except at the first and the last layers adjacent to the bottom and top walls, for which the second-order forward and the backward difference approximations are used, respectively. The second term on the RHS of Eq. (28) represents the divergence of diffusive fluxes of the free segment probability $P_{\mathbf{r}}^{\alpha}$ due to hops into and out of the control volume from/into adjacent unit cells, as shown in Fig. 3 in the case of a triangular lattice, for simplicity. The net diffusive flux of free segments of species α across each bond is given by

$$\mathbf{j}_{\mathbf{r},\mathbf{r}+\mathbf{a}_k}^{\alpha} = (1-\delta_{(\mathbf{r}+\mathbf{a}_k)\cdot\mathbf{e}_3,0})(1-\delta_{(\mathbf{r}+\mathbf{a}_k)\cdot\mathbf{e}_3,z_L+\sqrt{2/3}a})\left[\frac{D_{\mathbf{r},\mathbf{r}+\mathbf{a}_k}^{\alpha}}{(1-\bar{\phi})}\right] \times \left[P_{\mathbf{r}}^{\alpha}(1-\phi_{\mathbf{r}+\mathbf{a}_k})\varphi\left(\frac{\Delta_{\mathbf{r},\mathbf{r}+\mathbf{a}_k}\langle\mathcal{H}_{\mathbf{r}}^{\alpha}\rangle}{k_BT}\right) - P_{\mathbf{r}+\mathbf{a}_k}^{\alpha}(1-\phi_{\mathbf{r}})\varphi\left(-\frac{\Delta_{\mathbf{r},\mathbf{r}+\mathbf{a}_k}\langle\mathcal{H}_{\mathbf{r}}^{\alpha}\rangle}{k_BT}\right)\right]\frac{\mathbf{a}_k}{a}. \tag{29}$$

It is assumed that there are no fluxes coming into or out of the walls. The factors $(1-\delta_{(\mathbf{r}+\mathbf{a}_k)\cdot\mathbf{e}_3,0})$ and $(1-\delta_{(\mathbf{r}+\mathbf{a}_k)\cdot\mathbf{e}_3,z_L+\sqrt{2/3}a})$ suppress any contributions to fluxes from bottom and top walls, respectively. The net flux across a bond consists of the finite difference gradient of the probability current due to activated hops between the two adjacent sites. Consider a Markov chain model for the hopping flux from site $\mathbf{r}$ to site $\mathbf{r}+\mathbf{a}_k$. It is given by the product of the initial probability $P_{\mathbf{r}}^{\alpha}$ for the site $\mathbf{r}$ to be occupied by a free segment and the transition rate $[D_{\mathbf{r},\mathbf{r}+\mathbf{a}_k}^{\alpha}/(1-\bar{\phi})](1-\phi_{\mathbf{r}+\mathbf{a}_k})\varphi(\Delta_{\mathbf{r},\mathbf{r}+\mathbf{a}_k}\langle\mathcal{H}_{\mathbf{r}}^{\alpha}\rangle/k_BT)$ to hop from $\mathbf{r}$ to $\mathbf{r}+\mathbf{a}_k$. This transition rate vanishes if the site $\mathbf{r}+\mathbf{a}_k$ is not vacant. This is assured by the factor $(1-\phi_{\mathbf{r}+\mathbf{a}_k})$, which is the probability that the site $\mathbf{r}+\mathbf{a}_k$ is not occupied by a segment, including intrachain correlations in a chain of N^{α} freely jointed Kuhn segments. As discussed before, intrachain correlation effects are pronounced near walls and interfaces, where chain conformations are constrained. Note that $\phi_{\mathbf{r}}^{\alpha}=P_{\mathbf{r}}^{\alpha}$ in homogeneous or simple (monomer) fluids. For simple fluids [3,4], this form of diffusive fluxes is identical to the diffusive fluxes used in kinetic mean field theories [11] modeling diffusive hopping transport in stochastic lattice gases [93–95,102]. Since hopping is an activated rate process, the transition rate is proportional to $\varphi(\Delta_{\mathbf{r},\mathbf{r}+\mathbf{a}_k}\langle\mathcal{H}_{\mathbf{r}}^{\alpha}\rangle/k_BT)$, where the form of the rate function φ realizes a particular coupling to a heat bath. As a necessary condition to achieve convergence of the dynamic model to an equilibrium state under equilibrium conditions, the rate function has to satisfy the so-called local detailed balance relation [95]

$$\varphi(h) = e^{-h}\varphi(-h). \tag{30}$$

In our computation we use the Kawasaki form for the rate function (see discussion of this choice below)

$$\varphi(h) = \frac{2e^{-h/2}}{e^{h/2}+e^{-h/2}}. \tag{31}$$

This form of the transition rate function is certainly not unique [11,95]. There are many possible functional forms of the transition rate function satisfying Eq. (30), reflecting the many different possible realizations of the couplings to the heat bath in real systems. This is a well-known problem, which is by no means limited to the particular method for modeling nonequilibrium dynamics chosen here. For example, in the Langevin approach a particular coupling to the heat bath is realized by the functional form of the fluctuating noise term. As a necessary condition for converging to an equilibrium state under equilibrium conditions, the noise term has to satisfy the fluctuation-dissipation theorem, but there are many different forms of the noise term satisfying it. Similarly, there is a multitude of different methods for thermostating MD simulations, which have to satisfy some necessary conditions to reproduce equilibrium statistics under equilibrium conditions, but may lead to distinct nonequilibrium evolution.

In practice, it is found that, as long as detailed balance is satisfied, different realizations of the coupling to the heat bath may certainly affect the short-time and small-scale details of the dynamics, but recover similar qualitative trends at longer times and large scales. Hence the choice of a particular realization of the coupling to the heat bath in a nonequilibrium model is guided by simplifying assumptions idealizing such couplings in real systems, in order to make modeling practical. For example, in the Langevin approach a δ-function form for the "white" noise is commonly used for

analytical calculations, while a finite Gaussian form may be used in simulations. For kinetic lattice gases, the simplest analytical form for the transition rate function that satisfies Eq. (30) is $\varphi(h)=e^{-h/2}$. However, since it is not bounded in the limit $h\to-\infty$, it may cause frequent crashes in computer simulations due to overflows. The Metropolis form $\varphi(h)=\min\{1,e^{-h/2}\}$ is bounded, and indeed has been used extensively in Monte Carlo simulations, but its derivative has a discontinuity at $h=0$. This may not be important in Monte Carlo simulations, where the discontinuity is smeared by fluctuations, but it may cause stability problems when solving the mean field ordinary differential equations. The Kawasaki form of the rate function in Eq. (31) satisfies the local detailed balance relation (30), is bounded between 0 and 2, and is a smooth function.

The argument of the transition rate function $\Delta_{\mathbf{r},\mathbf{r}+\mathbf{a}_k}\langle\mathcal{H}^\alpha_{\mathbf{r}}\rangle/k_BT$ represents the change in the self-consistent potential field $\langle\mathcal{H}^\alpha_{\mathbf{r}}\rangle$ at site $\mathbf{r}$ that is caused by a hop of a single α-type Kuhn segment from site $\mathbf{r}$ to an adjacent vacant site $\mathbf{r}+\mathbf{a}_k$. Note that in a homogeneous system at thermodynamic equilibrium, the quantities $P^\alpha_{\mathbf{r}}$, $\phi^\alpha_{\mathbf{r}}$, $\langle\mathcal{H}^\alpha_{\mathbf{r}}\rangle$, and $D^\alpha_{\mathbf{r},\mathbf{r}+\mathbf{a}_k}$ are independent of $\mathbf{r}$ and $\mathbf{a}_k$, and $\Delta_{\mathbf{r},\mathbf{r}+\mathbf{a}_k}\langle\mathcal{H}^\alpha_{\mathbf{r}}\rangle=0$. Therefore the net diffusive currents across each bond vanish in such a system. We also know that $\phi^\alpha_{\mathbf{r}}$, $\langle\mathcal{H}^\alpha_{\mathbf{r}}\rangle$, and $D^\alpha_{\mathbf{r},\mathbf{r}+\mathbf{a}_k}$ are nonlinear functions of $P^\alpha_{\mathbf{r}}$. Consider small composition perturbations from an equilibrium homogeneous state far from the wall, while constraining the velocity field $\mathbf{u}_{\mathbf{r}}$ to be uniform. Noting that $1-\phi_{\mathbf{r}}=1-\bar{\phi}$ and $\varphi(0)=1$ in Eq. (31), Eq. (29) assumes the form

$$\mathbf{j}^\alpha_{\mathbf{r},\mathbf{r}+\mathbf{a}_k}=-D^\alpha_{\mathbf{r},\mathbf{r}+\mathbf{a}_k}\left(\frac{P^\alpha_{\mathbf{r}+\mathbf{a}_k}-P^\alpha_{\mathbf{r}}}{a}\right)\mathbf{a}_k, \tag{32}$$

which is similar to Fick's first law. Since the time evolution of $\phi^\alpha_{\mathbf{r}}$ is determined by the time evolution of $P^\alpha_{\mathbf{r}}$, we identify $D^\alpha_{\mathbf{r},\mathbf{r}+\mathbf{a}_k}$ with the translational self-diffusion coefficient D^α in the homogeneous equilibrium melt of homopolymer species α, given by the Stokes-Einstein relation

$$D^\alpha=\frac{k_BT}{N^\alpha\zeta^\alpha}, \tag{33}$$

where $N^\alpha\zeta^\alpha$ is the chain friction coefficient, and ζ^α is the segmental friction coefficient. For an inhomogeneous nonequilibrium system we assume

$$D^\alpha_{\mathbf{r},\mathbf{r}+\mathbf{a}_k}=\frac{k_BT}{N^\alpha\zeta^\alpha_{\mathbf{r},\mathbf{r}+\mathbf{a}_k}}, \tag{34}$$

where $\zeta^\alpha_{\mathbf{r},\mathbf{r}+\mathbf{a}_k}=\sqrt{\zeta^\alpha_{\mathbf{r}}\zeta^\alpha_{\mathbf{r}+\mathbf{a}_k}}$ is the geometric average of the local segmental friction coefficients at the two sites $\mathbf{r}$ and $\mathbf{r}+\mathbf{a}_k$. For a polymer melt above its glass transition, it is well known that local friction coefficients have a strong dependence on the local free volume $1-\phi_{\mathbf{r}}$. This dependence is captured by the Doolittle law [103]

$$\zeta^\alpha_{\mathbf{r}}=\zeta^\alpha_0\exp[(1-\phi_{\mathbf{r}})^{-1}-(1-\bar{\phi})], \tag{35}$$

where ζ^α_0 is the friction coefficient in a homogeneous melt at the reference temperature and pressure, whose density is $\bar{\phi}=\bar{\phi}(T_{ref},P_{ref})$. Note that Eq. (35) recovers the Doolittle law for the free volume relaxation time $\tau_f=\tau_0e^{1/f}$ in a system with homogeneous distribution of free volume $f=1-\bar{\phi}$. The Doolittle law is equivalent to the Vogel-Fulcher-Tammann-Hesse relation [104–107] and to the Williams-Landel-Ferry equation [108,109], and thus ensures recovery of the time-temperature superposition in a homogeneous system.

Within the framework of a dynamic self-consistent mean field approximation described above, a Kuhn segment of type α occupying the lattice site $\mathbf{r}$ interacts with a self-consistent potential field $\langle\mathcal{H}^\alpha_{\mathbf{r}}\rangle$ of the following form, when measured in units of k_BT:

$$\frac{\langle\mathcal{H}^\alpha_{\mathbf{r}}\rangle}{k_BT}=\frac{1}{2}\sum_\beta(1-\delta_{\alpha\beta})\chi_{\alpha\beta}\langle\langle\phi^\beta_{\mathbf{r}}\rangle\rangle+\chi^\alpha_s(\delta_{z,z_1}+\delta_{z,z_L})+\frac{m^\alpha}{2k_BT}\phi^\alpha_{\mathbf{r}}\mathbf{u}^2_{\mathbf{r}}+\frac{f^\alpha_{\mathbf{r}}w}{k_BT}. \tag{36}$$

The first term on the RHS of the equation above accounts for pair interactions with Kuhn segments at adjacent sites. These interactions are characterized by the segment-segment interaction parameter $\chi_{\alpha\beta}$, which is related to the Flory-Huggins [67] interaction parameter $12\chi_{\alpha\beta}$, defined as the energy change (normalized by k_BT) due to the transfer of an α segment from a melt of pure α to a melt of pure β. For segments of the same size, it is assumed that $\chi_{AA}=\chi_{BB}=0$ and that $\chi_{AB}=\chi_{BA}$. Within a mean field approximation [72–74], the form of the segment-segment contribution to the self-consistent potential field is obtained by averaging over all contacts that an α-type segment, located at site $\mathbf{r}$, has with segments of type β, located at sites $\mathbf{r}+\mathbf{a}_k$. We use the double angular brackets to denote summation over all nearest neighbors. Therefore, for the fcc lattice between the two walls we have

$$\langle\langle\phi^\beta_{\mathbf{r}}\rangle\rangle=\sum_{k=1}^{6}\phi^\beta_{\mathbf{r}+\mathbf{a}_k}+\sum_{k=7}^{9}(1-\delta_{z,z_L})\phi^\beta_{\mathbf{r}+\mathbf{a}_k}+\sum_{k=10}^{12}(1-\delta_{z,z_1})\phi^\beta_{\mathbf{r}+\mathbf{a}_k}. \tag{37}$$

Note that, since the segments at adjacent sites belong to freely jointed chains of Kuhn segments, the probabilistic averaging over segmental occupancies at the adjacent sites uses segmental volume fractions $\phi^\beta_{\mathbf{r}+\mathbf{a}_k}$ at these sites, rather than free segment probabilities $P^\beta_{\mathbf{r}+\mathbf{a}_k}$, to account for intrachain correlations. Thus the self-consistent computation of the potential field at site $\mathbf{r}$ is nonlocal, since it depends on segmental volume fractions $\phi^\beta_{\mathbf{r}+\mathbf{a}_k}$ at adjacent sites. This is true even for monomer fluids, where $\phi^\alpha_{\mathbf{r}}=P^\alpha_{\mathbf{r}}$. For polymer fluids, the self-consistent field calculation at site $\mathbf{r}$ involves $P^\alpha_{\mathbf{r}'}$ at even more remote sites. This is a consequence of Eq. (8), which relates the segmental volume fraction $\phi^\alpha_{\mathbf{r}}$ at site $\mathbf{r}$ to free segment probabilities $P^\alpha_{\mathbf{r}'}$ at all sites $\mathbf{r}'$ within a sphere about the site $\mathbf{r}$, with its radius being the extended length of the freely jointed chain.

The second term on the right-hand side of Eq. (36) represents interactions between the segments in the first and the last layers and the solid walls. The wall interaction parameter

χ_s^α is defined as the energy change (normalized by k_BT) due to the transfer of an α segment from a layer adjacent to a wall to a layer further away from the wall, in a pure fluid of α-type segments. It is negative for attractive segment-wall interactions, and positive for repulsive segment-wall interactions.

The first two terms in Eq. (36) are the familiar segmental interaction terms, which have the same form as in the equilibrium lattice SCF theory of Scheutjens and Fleer [12]. The last two terms make a nontrivial (i.e., nonconstant) contribution to the self-consistent potential only if the system is driven out of thermodynamic equilibrium by applied stresses, establishing a nonuniform velocity field $\mathbf{u_r}$, which, in turn, perturbs the conformation tensor $\mathbf{S}_\mathbf{r}^\alpha$ corresponding to the second moment of the end-to-end distance of ideal jointed chains from its equilibrium isotropic form. The third term is the kinetic energy contribution arising from the local mass averaged velocity of segments advected by the flow, based on the local equilibrium approximation defined in Eq. (3). A similar term arises in a dynamic self-consistent mean field theory for simple fluids [3,4]. The last term is not present in simple (monomer) fluids. It accounts for the local contribution to the free energy due to the deformation of polymer chains by the nonuniform flow, and is given by [10]

$$f_\mathbf{r}^\alpha = \tilde{u}_\mathbf{r} - T\tilde{s}_\mathbf{r} = -n_\mathbf{r}^\alpha k_BT \int \psi_\mathbf{r}^\alpha [\ln \psi_{\mathbf{r},0}^\alpha - \ln \psi_\mathbf{r}^\alpha] d\mathbf{Q}_\mathbf{r}^\alpha. \quad (38)$$

Here $n_\mathbf{r}^\alpha = (\phi_\mathbf{r}^\alpha w^{-1})/N^\alpha$ is the number density of α-type chains, $\tilde{u}_\mathbf{r}$ is the local internal energy of the polymer chains per unit volume, defined by the elastic potential energy of the springs in the FENE-P model, $\tilde{s}_\mathbf{r}$ is the configurational contribution of the chains to the entropy per unit volume, $\psi_\mathbf{r}^\alpha(\mathbf{Q}_\mathbf{r}^\alpha)$ is the local time-dependent probability distribution for finding a chain of type α with the center of mass at site $\mathbf{r}$ and the end-to-end distance $\mathbf{Q}_\mathbf{r}^\alpha$, given by Eq. (20), and $\psi_{\mathbf{r},0}^\alpha(\mathbf{Q}_\mathbf{r}^\alpha)$ is $\psi_\mathbf{r}^\alpha(\mathbf{Q}_\mathbf{r}^\alpha)$ at equilibrium. Evaluating the integral in Eq. (38) we get [10]

$$\frac{f_\mathbf{r}^\alpha}{k_BT} = -\frac{1}{2} n_\mathbf{r}^\alpha \left\{ \mathrm{Tr}\left(\boldsymbol{\delta} - \frac{3}{(N^\alpha - 1)a^2} \mathbf{S}_\mathbf{r}^\alpha \right) + \ln\left[\det\left(\frac{3}{(N^\alpha - 1)a^2} \mathbf{S}_\mathbf{r}^\alpha \right) \right] \right\}. \quad (39)$$

3. Time evolution of momentum density

Let us consider first the time evolution of momentum density in an incompressible homogeneous system of ideal (noninteracting) chains of type α that are modeled as FENE-P dumbbells. The time evolution of the second moment of the end-to-end vector for ideal dumbbells is given by Eq. (15), which we rewrite as follows:

$$\overset{\nabla}{\mathbf{S}}{}_\mathbf{r}^\alpha = -\frac{1}{\tau_{db,\mathbf{r}}^\alpha} \left(\frac{\mathbf{S}_\mathbf{r}^\alpha}{M_\mathbf{r}^\alpha} - \frac{(N^\alpha - 1)\tilde{a}_\alpha^2}{3} \boldsymbol{\delta} \right), \quad (40)$$

where

$$M_\mathbf{r}^\alpha = 1 - \frac{3}{(N^\alpha - 1)\tilde{a}_\alpha^2 b^\alpha} \mathrm{Tr}\mathbf{S}_\mathbf{r}^\alpha \quad (41)$$

originates from the nonlinear spring force in the FENE-P model ($M_\mathbf{r}^\alpha = 1$ in the Hookean dumbbell model that is recovered in the limit $b^\alpha \to \infty$) and $\tau_{db,\mathbf{r}}^\alpha$ is the local relaxation time for a Hookean dumbbell. Multiplication of Eq. (40) by $\tilde{\tau}_{db,\mathbf{r}}^\alpha = \tau_{db,\mathbf{r}}^\alpha M_\mathbf{r}^\alpha$ and rearrangement of the resulting equation gives

$$\tilde{\tau}_{db,\mathbf{r}}^\alpha \overset{\nabla}{\mathbf{S}}{}_\mathbf{r}^\alpha + \mathbf{S}_\mathbf{r}^\alpha = \frac{(N^\alpha - 1)\tilde{a}_\alpha^2}{3} M_\mathbf{r}^\alpha \boldsymbol{\delta}. \quad (42)$$

Let us define a *deviatoric* chain conformation tensor as follows:

$$\mathbf{T}_\mathbf{r}^\alpha = \mathbf{S}_\mathbf{r}^\alpha - \frac{(N^\alpha - 1)\tilde{a}_\alpha^2}{3} M_\mathbf{r}^\alpha \boldsymbol{\delta}. \quad (43)$$

Using Eq. (43) to find $\mathbf{S}_\mathbf{r}^\alpha$ as a function of $\mathbf{T}_\mathbf{r}^\alpha$, and substituting it into Eq. (42), we obtain

$$\tilde{\tau}_{db,\mathbf{r}}^\alpha \left(\overset{\nabla}{\mathbf{T}}{}_\mathbf{r}^\alpha + \frac{(N^\alpha - 1)\tilde{a}_\alpha^2}{3} \overset{\nabla}{(M_\mathbf{r}^\alpha \boldsymbol{\delta})} \right) + \mathbf{T}_\mathbf{r}^\alpha = 0, \quad (44)$$

where

$$\overset{\nabla}{(M_\mathbf{r}^\alpha \boldsymbol{\delta})} = \overset{\nabla}{M_\mathbf{r}^\alpha} \boldsymbol{\delta} + \frac{\partial M_\mathbf{r}^\alpha}{\partial t} \boldsymbol{\delta} + (\mathbf{u_r} \cdot \boldsymbol{\nabla} M_\mathbf{r}^\alpha) \boldsymbol{\delta}. \quad (45)$$

The upper-convective time derivative of the unit tensor is given by

$$\overset{\nabla}{\boldsymbol{\delta}} = \frac{D\boldsymbol{\delta}}{Dt} - \boldsymbol{\nabla}\mathbf{u}_\mathbf{r}^\mathrm{T} \cdot \boldsymbol{\delta} - \boldsymbol{\delta} \cdot \boldsymbol{\nabla}\mathbf{u_r} = -2\mathbf{D_r}, \quad (46)$$

where

$$\mathbf{D_r} = \frac{1}{2}(\boldsymbol{\nabla}\mathbf{u_r} + \boldsymbol{\nabla}\mathbf{u}_\mathbf{r}^\mathrm{T}) \quad (47)$$

is the rate-of-deformation tensor (i.e., the symmetric part of the velocity gradient).

Substituting Eq. (45) into Eq. (44) and using Eq. (46) yields the following expression for the deviatoric chain conformation tensor:

$$\mathbf{T}_\mathbf{r}^\alpha = 2\tilde{\tau}_{db,\mathbf{r}}^\alpha \frac{(N^\alpha - 1)\tilde{a}_\alpha^2}{3} M_\mathbf{r}^\alpha \mathbf{D_r} - \tilde{\tau}_{db,\mathbf{r}}^\alpha \left[\overset{\nabla}{\mathbf{T}}{}_\mathbf{r}^\alpha + \frac{(N^\alpha - 1)\tilde{a}_\alpha^2}{3} \left(\frac{\partial M_\mathbf{r}^\alpha}{\partial t} \boldsymbol{\delta} + (\mathbf{u_r} \cdot \boldsymbol{\nabla} M_\mathbf{r}^\alpha) \boldsymbol{\delta} \right) \right], \quad (48)$$

If $n_\mathbf{r}^\alpha$ is the local number density of ideal (noninteracting) FENE-P chains of type α at site $\mathbf{r}$, their contribution to the stress is

$$\boldsymbol{\sigma}_\mathbf{r}^\alpha = n_\mathbf{r}^\alpha \frac{3k_BT}{M_\mathbf{r}^\alpha (N^\alpha - 1)\tilde{a}_\alpha^2} \mathbf{S}_\mathbf{r}^\alpha, \quad (49)$$

where the chain number density $n_\mathbf{r}^\alpha$ is constant in an incom-

pressible system. The contribution of these chains to the *deviatoric* stress tensor at site $\mathbf{r}$ is defined as

$$\boldsymbol{\tau}_{\mathbf{r}}^{\alpha} = n_{\mathbf{r}}^{\alpha} \frac{3k_B T}{M_{\mathbf{r}}^{\alpha}(N^{\alpha}-1)\tilde{a}_{\alpha}^2} \mathbf{T}_{\mathbf{r}}^{\alpha}. \tag{50}$$

Multiplying Eq. (48) by $n_{\mathbf{r}}^{\alpha}[3k_B T/M_{\mathbf{r}}^{\alpha}(N^{\alpha}-1)\tilde{a}_{\alpha}^2]$, and using $\tau_{db,\mathbf{r}}^{\alpha} = \tilde{\tau}_{db,\mathbf{r}}^{\alpha}/M_{\mathbf{r}}^{\alpha}$ and Eq. (18) defining the Hookean relaxation time $\tau_{db,\mathbf{r}}^{\alpha}$, we obtain

$$\boldsymbol{\tau}_{\mathbf{r}}^{\alpha} = 2\eta_{\mathbf{r}}^{\alpha}\mathbf{D}_{\mathbf{r}} - \boldsymbol{\varepsilon}_{\mathbf{r}}^{\alpha}, \tag{51}$$

where

$$\boldsymbol{\varepsilon}_{\mathbf{r}}^{\alpha} = \frac{n_{\mathbf{r}}^{\alpha} N^{\alpha} \zeta_{\mathbf{r}}^{\alpha}}{8} \left[\overset{\nabla}{\mathbf{T}}_{\mathbf{r}}^{\alpha} \frac{(N^{\alpha}-1)\tilde{a}_{\alpha}^2}{3} \left(\frac{\partial M_{\mathbf{r}}^{\alpha}}{\partial t}\boldsymbol{\delta} + (\mathbf{u}_{\mathbf{r}} \cdot \nabla M_{\mathbf{r}}^{\alpha})\boldsymbol{\delta} \right) \right], \tag{52}$$

and both $n_{\mathbf{r}}^{\alpha}$ and $\zeta_{\mathbf{r}}^{\alpha}$ are constant in an incompressible system. In Eq. (52),

$$\eta_{\mathbf{r}}^{\alpha} = \tilde{\tau}_{db,\mathbf{r}}^{\alpha} G_{\mathbf{r}}^{\alpha} = n_{\mathbf{r}}^{\alpha} M_{\mathbf{r}}^{\alpha} N^{\alpha}(N^{\alpha}-1)\zeta_{\mathbf{r}}^{\alpha}\tilde{a}_{\alpha}^2/24 \tag{53}$$

is the contribution to the local shear viscosity in a system of ideal chains of type α with local density $n_{\mathbf{r}}^{\alpha}$. Here $G_{\mathbf{r}}^{\alpha} = n_{\mathbf{r}}^{\alpha} k_B T$ is the chain contribution to the bulk modulus and $\tilde{\tau}_{db,\mathbf{r}}^{\alpha}$ is the effective relaxation time for FENE-P dumbbells. Thus the first term on the RHS of Eq. (51) is a Newtonian viscous contribution to the deviatoric stress. The second term on the RHS of Eq. (51) vanishes for a homogeneous system at the steady state. We will refer to it as the *elastic* contribution to the deviatoric stress. The time evolution of the momentum density of segments belonging to a melt of ideal chains of type α is given by

$$\frac{d\mathbf{g}_{\mathbf{r}}^{\alpha}}{dt} = \nabla \cdot (-\mathbf{g}_{\mathbf{r}}^{\alpha}\mathbf{u}_{\mathbf{r}} - \boldsymbol{\varepsilon}_{\mathbf{r}}^{\alpha} + 2\eta_{\mathbf{r}}^{\alpha}\mathbf{D}_{\mathbf{r}}), \tag{54}$$

where $-\mathbf{g}_{\mathbf{r}}^{\alpha}\mathbf{u}_{\mathbf{r}}$, $-\boldsymbol{\varepsilon}_{\mathbf{r}}^{\alpha}$, and $2\eta_{\mathbf{r}}^{\alpha}\mathbf{D}_{\mathbf{r}}$ are the convective, elastic, and viscous contributions to the stress, respectively. Note that for a one-component incompressible fluid, where $\rho_{\mathbf{r}}^{\alpha}$ and $\eta_{\mathbf{r}}^{\alpha}$ are constant, $\nabla \cdot \mathbf{u}_{\mathbf{r}} = 0$, and $\mathbf{g}_{\mathbf{r}}^{\alpha} = \rho_{\mathbf{r}}^{\alpha}\mathbf{u}_{\mathbf{r}}^{\alpha}$. The viscous term represents diffusion of the momentum density components, as seen from the following

$$\nabla \cdot (2\eta_{\mathbf{r}}^{\alpha}\mathbf{D}_{\mathbf{r}}) = \eta_{\mathbf{r}}^{\alpha} \nabla \cdot (\nabla \mathbf{u}_{\mathbf{r}} + \nabla \mathbf{u}_{\mathbf{r}}^{T}) = \nu_{\mathbf{r}}^{\alpha} \nabla^2 \mathbf{g}_{\mathbf{r}}^{\alpha}, \tag{55}$$

where the kinematic viscosity $\nu_{\mathbf{r}}^{\alpha} = \eta_{\mathbf{r}}^{\alpha}/\rho_{\mathbf{r}}^{\alpha}$ plays the role of a diffusion coefficient for propagation of momentum.

We postulate here that in real (compressible) inhomogeneous fluids this term is caused by hopping of segments from an occupied cage to an adjacent vacant one. Such a postulate was used in the DSCF theory for simple (monomer) fluids of Khan and Shnidman, which produced detailed computations of interfacial and wetting flows. However, the concept of viscous momentum propagation by activated hopping can be traced all the way back to the classic kinetic theories of liquids by Eyring [1] and Frenkel [2].

Applying the postulate above to an inhomogeneous, compressible blend of chains of two types $\alpha = A, B$, interacting with each other and with the walls according to the self-consistent model (37), Eq. (54) is replaced by the following equation for the evolution of momentum density at site $\mathbf{r}$:

$$\frac{d\mathbf{g}_{\mathbf{r}}^{\alpha}}{dt} = -\nabla \cdot (\mathbf{g}_{\mathbf{r}}^{\alpha}\mathbf{u}_{\mathbf{r}} + \boldsymbol{\varepsilon}_{\mathbf{r}}^{\alpha}) - \sum_{k=1}^{12} \frac{\boldsymbol{\pi}_{\mathbf{r},\mathbf{r}+\mathbf{a}_k}^{\alpha}}{a} - \frac{\phi_{\mathbf{r}}^{\alpha}}{wP_{\mathbf{r}}^{\alpha}} \sum_{k=1}^{12} \zeta_{\mathbf{r},\mathbf{r}+\mathbf{a}_k}^{\alpha} \mathbf{j}_{\mathbf{r},\mathbf{r}+\mathbf{a}_k}^{\alpha}. \tag{56}$$

The term $\mathbf{g}_{\mathbf{r}}^{\alpha}\mathbf{u}_{\mathbf{r}}$ in Eqs. (54) and (56) represents the convective contribution to the stress, and is unchanged. However, note that now $\mathbf{u}_{\mathbf{r}}$ is the mass-averaged mean velocity, as given by Eq. (14). The term $-\boldsymbol{\varepsilon}_{\mathbf{r}}^{\alpha}$ in Eq. (56) represents the elastic contribution to the stress and is still given by Eq. (52), except that $n_{\mathbf{r}}^{\alpha}$ and $\zeta_{\mathbf{r}}^{\alpha}$ are now functions of $\mathbf{r}$.

The divergence of the viscous stress $\nabla \cdot (2\eta_{\mathbf{r}}^{\alpha}\mathbf{D}_{\mathbf{r}})$ in Eq. (54) is replaced by the term $\Sigma_k \boldsymbol{\pi}_{\mathbf{r},\mathbf{r}+\mathbf{a}_k}^{\alpha}/a$ in Eq. (56), using a Markov chain model for activated-rate viscous transport of momentum between adjacent sites. The net change $-\boldsymbol{\pi}_{\mathbf{r},\mathbf{r}+\mathbf{a}_k}^{\alpha}/a$ in local momentum density due to hopping of segments of species α across each bond between adjacent sites $\mathbf{r}$ and $\mathbf{r}+\mathbf{a}_k$ is given by

$$\begin{aligned} \boldsymbol{\pi}_{\mathbf{r},\mathbf{r}+\mathbf{a}_k}^{\alpha} = {} & (1-\delta_{(\mathbf{r}+\mathbf{a}_k)\cdot\mathbf{e}_3,0})(1-\delta_{(\mathbf{r}+\mathbf{a}_k)\cdot\mathbf{e}_3,z_L+\sqrt{2/3}a}) \frac{\nu_{\mathbf{r},\mathbf{r}+\mathbf{a}_k}^{\alpha}}{(1-\bar{\phi})} \\ & \times \left[\mathbf{g}_{\mathbf{r}}^{\alpha}(1-\phi_{\mathbf{r}+\mathbf{a}_k}^{\alpha}) \varphi\left(\frac{\Delta_{\mathbf{r},\mathbf{r}+\mathbf{a}_k}\langle \mathcal{H}_{\mathbf{r}}^{\alpha} \rangle}{k_B T} \right) \right. \\ & \left. - \mathbf{g}_{\mathbf{r}+\mathbf{a}_k}^{\alpha}(1-\phi_{\mathbf{r}}^{\alpha}) \varphi\left(-\frac{\Delta_{\mathbf{r},\mathbf{r}+\mathbf{a}_k}\langle \mathcal{H}_{\mathbf{r}}^{\alpha} \rangle}{k_B T} \right) \right] \frac{\mathbf{a}_k}{a}. \end{aligned} \tag{57}$$

For each component of the segmental momentum density vector $\mathbf{g}_{\mathbf{r}}^{\alpha}$, Eq. (57) has the same form as Eq. (29), which defines diffusive free segment probability fluxes $\mathbf{j}_{\mathbf{r},\mathbf{r}+\mathbf{a}_k}^{\alpha}$, with components of segmental momentum density $\mathbf{g}_{\mathbf{r}}^{\alpha}$ replacing the free segment probability $P_{\mathbf{r}}^{\alpha}$, and the local kinematic shear viscosity coefficient at zero shear rate $\nu_{\mathbf{r},\mathbf{r}+\mathbf{a}_k}^{\alpha}/(1-\bar{\phi})$ replacing the local self-diffusion coefficient $D_{\mathbf{r},\mathbf{r}+\mathbf{a}_k}^{\alpha}/(1-\bar{\phi})$. In a FENE-P dumbbell model for the chain,

$$\nu_{\mathbf{r},\mathbf{r}+\mathbf{a}_k}^{\alpha} = \frac{\zeta_{\mathbf{r},\mathbf{r}+\mathbf{a}_k}^{\alpha} \tilde{a}_{\alpha}^2 M_{\mathbf{r}}^{\alpha}}{24 m^{\alpha}} \tag{58}$$

where $\zeta_{\mathbf{r},\mathbf{r}+\mathbf{a}_k}^{\alpha} = \sqrt{\zeta_{\mathbf{r}}^{\alpha}\zeta_{\mathbf{r}+\mathbf{a}_k}^{\alpha}}$ is the geometric average of the local segmental friction coefficients at sites $\mathbf{r}$ and $\mathbf{r}+\mathbf{a}_k$ obeying the Doolittle law [103] [Eq. (35)]. The transition rate function φ has been defined in Eq. (31). It depends on $\Delta_{\mathbf{r},\mathbf{r}+\mathbf{a}_k}\langle \mathcal{H}_{\mathbf{r}}^{\alpha} \rangle/k_B T$, the change in the self-consistent potential field at site $\mathbf{r}$ resulting from a segment of type α hopping from site $\mathbf{r}$ to an adjacent vacant site $\mathbf{r}+\mathbf{a}_k$. The dependence of $\langle \mathcal{H}_{\mathbf{r}}^{\alpha} \rangle/k_B T$ on segmental interactions (with segments of opposite type and with walls), local kinetic energy, and chain conformations has been described by Eqs. (36)–(39).

For a one-component, incompressible fluid, $1-\phi_{\mathbf{r}} = 1-\bar{\phi}$, and $\varphi(0) = 1$ in Eq. (31), and the kinematic viscosity coefficient $\nu_{\mathbf{r},\mathbf{r}+\mathbf{a}_k}^{\alpha} = \nu^{\alpha} = \eta^{\alpha}/\rho^{\alpha}$ is constant. In this case, we recover Newton's law for viscous contribution to the stress $-\boldsymbol{\pi}_{\mathbf{r},\mathbf{r}+\mathbf{a}_k}^{\alpha}$ arising from hops between sites $\mathbf{r}$ and $\mathbf{r}+\mathbf{a}_k$,

$$-\boldsymbol{\pi}^{\alpha}_{\mathbf{r},\mathbf{r}+\mathbf{a}_k} = \nu^{\alpha}\left(\frac{\mathbf{g}^{\alpha}_{\mathbf{r}+\mathbf{a}_k} - \mathbf{g}^{\alpha}_{\mathbf{r}}}{a}\right)\mathbf{a}_k = \eta^{\alpha}\left(\frac{\mathbf{u}_{\mathbf{r}+\mathbf{a}} - \mathbf{u}^{\alpha}_{\mathbf{r}}}{a}\right)\mathbf{a}_k. \quad (59)$$

The last term in Eq. (56) has no counterpart in Eq. (54). Its origin can be understood as follows. The probability density for a segment belonging to a chain of connected segments of type α is $\phi^{\alpha}_{\mathbf{r}}/w$. If $\mathbf{j}^{\alpha}_{\mathbf{r},\mathbf{r}+\mathbf{a}_k}$ is not zero, there is a net drift velocity $\mathbf{j}^{\alpha}_{\mathbf{r},\mathbf{r}+\mathbf{a}_k}/P^{\alpha}_{\mathbf{r}}$ due to biased hopping between the sites $\mathbf{r}$ and $\mathbf{r}+\mathbf{a}_k$. This contributes $(\phi^{\alpha}_{\mathbf{r}}/w)(-\zeta^{\alpha}_{\mathbf{r},\mathbf{r}+\mathbf{a}_k}\mathbf{j}^{\alpha}_{\mathbf{r},\mathbf{r}+\mathbf{a}_k}/P^{\alpha}_{\mathbf{r}})$ to the friction force density, and the total friction force density is obtained by summing over all the bonds (it is negligible for an incompressible one-species fluid of ideal chains).

Our isothermal DSCF theory for unentangled polymer blends results in a system of coupled nonlinear ordinary differential equations for a set of independent variables defined at each site $\mathbf{r}$ on the fcc lattice: $P^{A}_{\mathbf{r}}$, $\mathbf{g}^{A}_{\mathbf{r}}$, and $\mathbf{S}^{A}_{\mathbf{r}}$ (one-component fluid), or $P^{A}_{\mathbf{r}}$, $P^{B}_{\mathbf{r}}$, $\mathbf{g}^{A}_{\mathbf{r}}$, $\mathbf{g}^{A}_{\mathbf{r}}$, $\mathbf{S}^{A}_{\mathbf{r}}$, and $\mathbf{S}^{B}_{\mathbf{r}}$ (two-component fluid). For systems exhibiting translational invariance within triangular layers parallel to the walls, the spatial computational grid becomes one dimensional. In order to solve these DSCF equations, one has to prescribe boundary conditions for $\mathbf{u}_{\mathbf{r}}=\mathbf{g}_{\mathbf{r}}/\rho_{\mathbf{r}}$ at sites adjoining the walls. We assume that if a connected segment of type α occupies a site $\mathbf{r}$ adjacent to a wall (which occurs with probability $\phi^{\alpha}_{\mathbf{r}}$), then it acquires the velocity of that wall. Therefore, for the geometry specified in Figs. 1 and 2, the mass-averaged mean velocity at the sites next to the walls is set to

$$\mathbf{u}_{z=z_1} = -\sum_{\alpha}\phi^{\alpha}_{z=z_1}u_w\mathbf{e}_1, \quad \mathbf{u}_{z=z_L} = \sum_{\alpha}\phi^{\alpha}_{z=z_1}u_w\mathbf{e}_1, \quad (60)$$

where $z_1 \equiv \sqrt{2/3}a$, $z_L \equiv \sqrt{2/3}aL$, and L is the number of triangular lattice layers stacked in a fcc lattice arrangement between the walls. Periodic boundary conditions are used in the directions perpendicular to the walls.

IV. ONE-COMPONENT MELTS

A. Simulation setup and parameter estimation

As our first application of the DSCF theory, we have studied the morphology and rheology of unentangled homopolymer melts consisting of a single component A in a sheared planar channel between two solid walls [see Fig. 1(a)]. We assume that the homopolymer chains in the melt are linear and unentangled. Furthermore, we assume that the melt stays invariant under translations in directions parallel to the walls, and is kept isothermal and isobaric at temperature $T=509$ K and atmospheric pressure. Each homopolymer chain is modeled by N^{α} freely jointed Kuhn segments. For the Kuhn segment length, we adopted the value $a=4.6$ Å used by Li and Ruckenstein [110] in their equilibrium SCF study of polyethylene chains. The lattice constant of the fcc lattice used in our DSCF model is assigned the value of the Kuhn length cited above. The molecular weight of a homopolymer melt is assumed to be below the entanglement molecular weight, $M<M_e$. This restricts the number of Kuhn segments in a homopolymer chain to $N^{\alpha}<N_e$, where N_e is the mean number of Kuhn segments between entanglements. The value of N_e has been controversial. Estimates in the literature [111] vary between 35 and 75. Since the present form of our DSCF model is limited to unentangled fluids, we conservatively limited the number of Kuhn segments in the homopolymer chains to $N^{\alpha}\leqslant 32$, which is below the lower bound for N_e cited above.

We used the Stokes-Einstein relation to determine the segmental friction coefficient from the value of the self-diffusion coefficient for an equilibrium polyethylene melt at the same temperature and pressure, obtained by Paul *et al.* [45] from MD simulations and neutron spin-echo spectroscopy. The free volume in the bulk of the melt is estimated from the difference between the densities of polyethylene at $T=509$ K and at the glass transition temperature $T_g=263$ K, both at atmospheric pressure. This leads to the estimate of the free volume fraction in the bulk phase of polyethylene melt at $T=509$ K and atmospheric pressure being $\bar{\phi}^0=1-\bar{\phi}=0.15$, where $\bar{\phi}=0.85$ is the volume fraction of polymer chains.

The DSCF theory is first used to equilibrate a homopolymer melt between static planar walls by solving the evolution equations with $\mathbf{g}^{A}_{\mathbf{r}}=\mathbf{u}_{\mathbf{r}}=\mathbf{0}$ at each site, using the isotropic equilibrium stepping probabilities $\lambda^{A}_{\mathbf{a}_k,\mathbf{r}}=\frac{1}{12}$ for all k. The equilibration run was always started from the homogeneous bulk phase values for polyethylene melt at $T=509$ K and atmospheric pressure. The results of the equilibration run provided the initial values for solving the DSCF evolution equations in a channel between an upper and a lower planar walls moving at constant velocities $\mathbf{u}_w=\pm u_w\mathbf{e}_1$, respectively, until a nonequilibrium steady state was reached. This corresponds to a constant nominal shear rate $\dot{\gamma}=2u_w/[\sqrt{2/3}(L+1)a]$, where $\sqrt{2/3}(L+1)a$ is the distance between the two walls containing L triangular lattice layers of Kuhn segments stacked in a fcc lattice arrangement. This procedure was repeated for a number of different values of $\dot{\gamma}$ and N^A. To investigate relaxation from a nonequilibrium steady state back to thermodynamic equilibrium, in some instances we furthermore used the steady-state results as initial values for solving the quasi-one-dimensional DSCF equations at $\dot{\gamma}=0$. The DSCF results reported below use a system of fundamental units consisting of [energy]$=k_BT$, [length]$=a$, and [time]$=\tau$, where $\tau=a^2/D^A_0$ is the characteristic time for a probe (unconnected) segment of type A to diffuse a distance a, and D^A_0 is the self-diffusion coefficient of the A-type probe segment, related to its friction coefficient ζ^A_0 by the Stokes-Einstein relation $D^A_0=k_BT/\zeta^A_0$. All the quantities obtained from the DSCF simulations reported below are expressed in these units.

B. DSCF simulation results for melts

In this subsection we report the results of DSCF simulations of a one-component homopolymer melt across a planar channel that is sheared at a nominal shear rate $\dot{\gamma}=1\times10^{-3}\tau^{-1}$. The channel contained $L=64$ triangular lattice layers stacked in the fcc lattice arrangement. We used linear chains of $N^A=24$ freely jointed Kuhn segments in the simulations reported in this subsection, unless stated other-

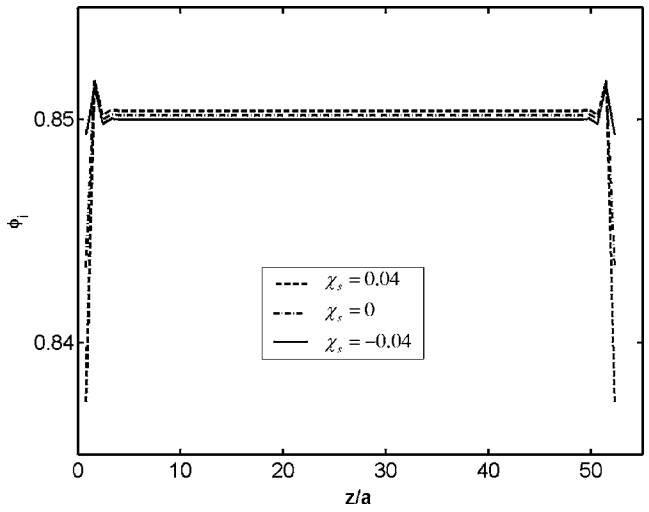

FIG. 4. Steady-state segmental volume fraction profiles of a one-component homopolymer melt, across the channel, obtained at a nominal shear rate $\dot{\gamma}=1\times10^{-3}\tau^{-1}$. The polymer chain consists of $N^A=24$ Kuhn segments. The short-range interactions between the polymer segments and the solid walls vary between attractive ($\chi_s<0$), neutral ($\chi_s=0$), and repulsive ($\chi_s>0$).

wise. Figure 4 shows the variation of segmental volume fraction ϕ_z across the channel. At this nominal shear rate, the segmental volume fraction profiles at nonequilibrium steady state are not discernible from the equilibrium profiles. The three profiles correspond to attractive ($\chi_s<0$), neutral ($\chi_s=0$), and repulsive ($\chi_s>0$) segment-wall interactions. Thus the depletion of polymer segmental volume fraction in the layers next to the solid wall is sensitive to the segment-wall interactions. The depletion at the wall is followed by a nonmonotonic, oscillatory approach toward bulk values, spanning the next few layers. If the system were infinite, the bulk values would correspond to the mean total volume fraction of the polymer fluid, $\bar{\phi}=0.85$. However the bulk densities deviate from $\bar{\phi}$, due to the finite size effects caused by the small separation between the wall and the segment-surface interactions.

Note that if the original equilibrium SCF lattice theory of Scheutjens and Fleer [68] were applied to a one-component melt at equilibrium between two static walls, the segmental volume fraction profile across the channel would be homogeneous, since their theory is incompressible. However, similar wall-depletion and finite-size effects are produced by compressible variants of the equilibrium Scheutjens-Fleer SCF theory [69–71]. It is also worth noting that a depleted layer adjacent to the wall also occurs in lattice gas models of simple liquids consisting of small molecules [3,4], if there is a strong repulsive interaction between the wall and the molecules in the adjacent layer. However, wall depletion of segmental volume fractions in polymer melts is predominantly caused by an entropic, rather than enthalpic effect, as the number of available chain conformations is reduced next to the walls. As shown in Fig. 4, wall depletion of segmental volume fractions in polymer melts occurs even when the walls are neutral ($\chi_s=0$), though it can be enhanced by repulsive wall interactions ($\chi_s>0$) and diminished by attractive interactions with the wall ($\chi_s<0$). The oscillatory decay of the depletion at increasing distances from the wall can be attributed to intrachain correlations between the segments. In all the other simulations reported here we used neutral walls ($\chi_s=0$).

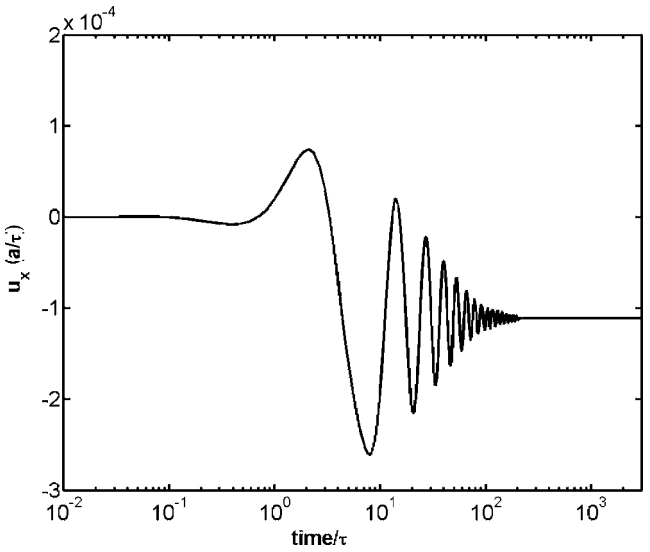

FIG. 5. Time evolution of the velocity in the lower quarter channel, obtained at a nominal shear rate $\dot{\gamma}=1\times10^{-5}\tau^{-1}$. The walls are neutral ($\chi_s=0$), and the chain length is $N^A=24$.

In Figs. 5 and 6 we analyze further the results of a DSCF simulation of the system with the same parameters as in Fig. 4, restricted to neutral ($\chi_s=0$) segmental interactions with the walls. We have studied the time evolution of the x component of the velocity in a planar channel between two sheared walls. Prior to initializing shear at $t=0$, the velocity of both walls and of the fluid between them was zero, corresponding to a system at thermal equilibrium. At subsequent times, we first observed rapid, nonmonotonic propagation of the momentum (and, therefore, of the velocity) from the wall. This

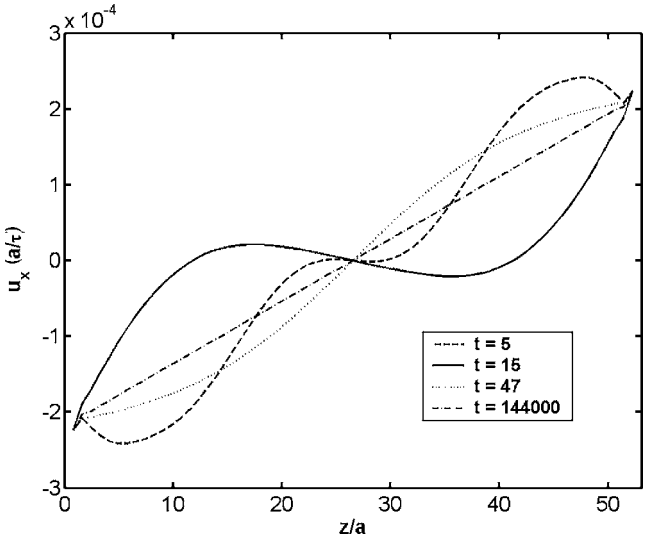

FIG. 6. Velocity profiles across the channel, given at selected times and at steady state (denoted by the dash-dotted line).

quasi-oscillatory behavior originated from $-\boldsymbol{\varepsilon}_i^{\alpha}$, the elastic contribution to the stress [see Eqs. (52), (53), and (55)], and it disappeared when the elastic contribution to the stress was neglected in the momentum evolution equations. In a continuum PDE model of a sheared incompressible non-Newtonian fluid [112], a similar elastic contribution to the stress introduces a term of hyperbolic nature into the momentum evolution, giving rise to shock waves which are smeared and damped by the viscous term. It is known that smearing of shock wave solutions to hyperbolic partial differential equations is enhanced by finite difference approximations of the type that we used here [113].

Figure 5 displays the time evolution of the x component of the velocity profile in a layer parallel to the walls located at a lower quarter channel. Note that we use a logarithmic time scale. Notice that at early times ($t \leqslant 10^{-1}\tau$), the velocity at the layer is zero, as momentum has not yet propagated to this layer. Between $t \approx 10^{-1}\tau$ and $t \approx 3 \times 10^{-1}\tau$ the x component of the velocity exhibits a slight undershoot, which may not be physical, but is rather an artifact of our finite difference approximation. After this time, the smeared velocity shock wave is reflected back and forth between the two channel walls, with the amplitude damped by the viscous term. Finally, around $t \approx 2 \times 10^{2}\tau$ the oscillations are completely damped out, and the x component of the velocity approaches its steady state value at this layer.

Figure 6 shows the wavelike propagation of the x component of the velocity across the channel at earlier times, and its subsequent damping by the viscous term in the momentum transport equation [the first sum on the RHS of Eq. (56)] resulting in a Couette-like steady-state profile at long times. This profile is linear across the channel, except near the walls, where we observe a noticeable velocity slip. We note that a velocity slip can be observed even in DSCF simulations of simple liquids of small molecules in a sheared capillary, if there is a strong unfavorable interaction between the molecules and the walls that leads to a depletion layer at the walls [3,4]. Such velocity slip effects have been known since Tolstoi's pioneering observations [114] on capillary flow of water in hydrophobic microcapillaries, and have been discussed extensively in the literature [115–117]. We believe that, in the case of polymer melts, the velocity slip at the wall (Fig. 6) is also caused by the depletion of the segmental volume fraction near the walls, as seen in Fig. 4, though in this case the depletion is dominated by the chain entropy effects mentioned above.

The time evolution of the shear stress, in a layer at the lower quarter channel, is shown in Fig. 7. The system is first equilibrated and then subjected to a steady shear flow (at a nominal shear rate $\dot{\gamma} = 1 \times 10^{-5}\tau^{-1}$). Figure 7(a) shows the development of the shear stress, at the layer located at the lower quarter of the channel, after the onset of shear. Until around $t \approx 7 \times 10^{-1}\tau$ the velocity has not propagated to this layer yet, and the shear stress is zero. After this time, a slight undershoot develops in the shear stress before it starts rising. However, as explained above, this behavior could be an artifact of our model. From this time on, the shear stress develops in the manner of a smeared shock wave with decaying amplitude. In the course of time, these shock waves are damped out by the viscous term, and the shear stress reaches its steady state value. This steady state is used as a starting point for a consecutive simulation in which the wall velocity is set to zero, and the system is allowed to relax. Figure 7(b) displays this stress relaxation. The shear stress initially retains its steady state value until the velocity at this layer starts to decay. The overshoot observed at $t \approx 7 \times 10^{-1}\tau - 2 \times 10^{0}\tau$ could be just an artifact as mentioned above. After this time, the shear stress decays in the fashion of a smeared shock wave, with the amplitude of the shock waves being damped viscously, until it vanishes.

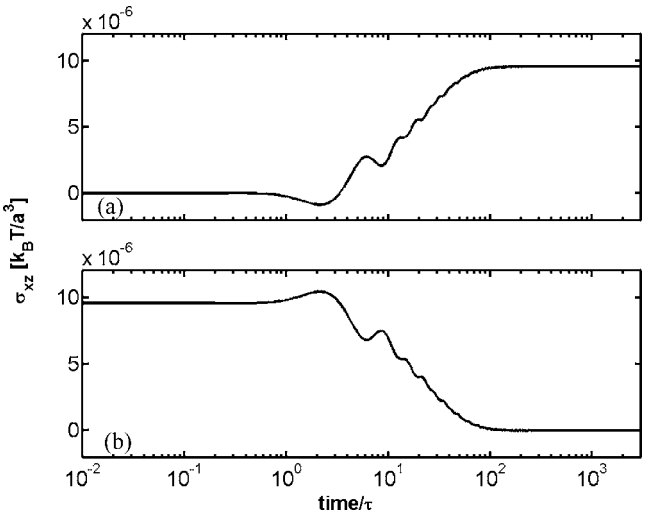

FIG. 7. Time evolution of the shear stress, at the lower quarter channel, following (a) the onset of a steady shear, and (b) the recession of the shear.

The extent to which an ideal (noninteracting) polymer test chain is stretched under a nonuniform flow velocity field can be quantified by calculating the eigenvalues of the tensor of the second moment of the end-to-end vector. The three eigenvalues quantify stretching along the three principal axes of this tensor. Figure 8 displays the time evolution, at a mid-channel layer, of the (a) largest, (b) intermediate, and (c) smallest eigenvalues, normalized by their equilibrium values. At the reported nominal shear rate $\dot{\gamma} = 1 \times 10^{-5}\tau^{-1}$, the stretching of the homopolymer ideal test chain consisting of $N^A = 24$ Kuhn segments is slight. However, note that, similarly to the time evolution of the flow velocity, both the highest and smallest eigenvalues seem to converge toward their steady-state values in a nonmonotonic, oscillatory fashion.

Figure 9(a) displays the time evolution of the first normal stress difference, defined by $N_1 = \sigma_{xx} - \sigma_{zz}$. Its positive value indicates that there is a higher degree of orientation in the flow direction (the x direction) than in the direction of the velocity gradient (the z direction). The four different curves in Fig. 9(a) correspond to four different chain lengths $N^A = 8$, 16, 24, and 32, showing the dependence of N_1 on the chain length. The other parameters have the same value as in Fig. 5 (with $\chi_s = 0$). The time-dependent growth of N_1 upon startup of steady shearing also follows a nonmonotonic, oscillatory trend, until N_1 converges to its steady state value. Figure 9(b) displays an enlarged view of the rise and decay of these oscillations.

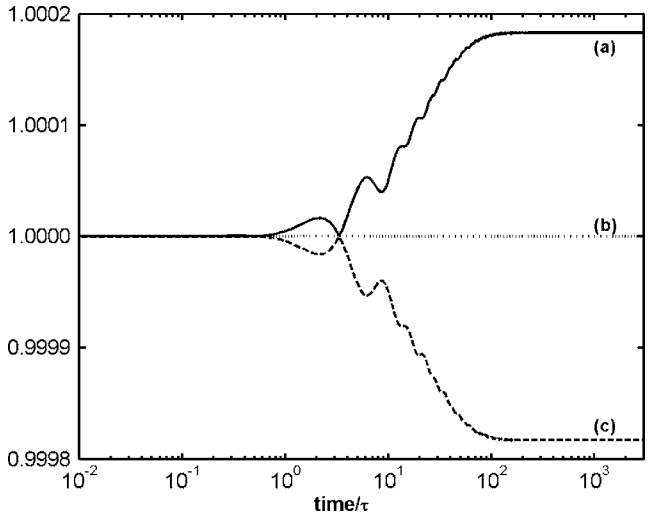

FIG. 8. Time evolution of the stretching of an ideal (noninteracting) polymer chain under flow (at $\dot{\gamma}=1\times10^{-5}\tau^{-1}$). The stretching is calculated using the (a) largest, (b) intermediate, and (c) smallest eigenvalues of the second moment of the end-to-end distance, normalized by their values at equilibrium.

V. PHASE-SEPARATED SYMMETRIC BLENDS

A. Simulation setup and parameter estimation

As the next application of our DSCF theory, we chose to simulate phase-separated, two-component homopolymer blends in a planar channel. We have assumed the same Kuhn segment length, glass transition temperature and bulk values of the density, friction coefficient and transport coefficients for the pure one-component phases of the two A and B species as for the one-component A melt in Sec. IV. The distance between the two walls, the temperature, and the nominal shear rate were also set at the same values as in Sec. IV, but the nominal shear rate was set at a much higher value $\dot{\gamma}=1\times10^{-3}\tau^{-1}$. The segment-wall interactions were assumed to be neutral ($\chi_s^A=\chi_s^B=0$) with respect to both species, and the segment-segment interaction parameter between both species was set at $\chi_{AB}=0.55/12$, corresponding to a Flory-Huggins interaction parameter $12\chi_{AB}=0.55$.

The two-component immiscible blend was first equilibrated by integrating the DSCF equations at zero wall velocities. The equilibration was initialized using a sharp step function profile of the segmental volume fraction of the two species across the channel, and resulted in a coexistence of a majority-A and a majority-B bulk phases, with smooth interfacial profiles of the segmental volume fractions of the two species across the interface between the two phases, as shown by the solid lines in Fig. 10. Using equilibrium results as an initial input at time $t=0$, the DSCF equations are then integrated for $t>0$ with the top and bottom wall velocities set to constant but opposite values $\mathbf{u}_w=\pm u_w\mathbf{e}_1$ corresponding to the chosen nominal shear rate.

B. Simulation results for immiscible blends

Figures 10–13 present the results of simulating the phase separated, two-component unentangled polymer blend in a sheared channel, using the parameters specified in Sec. V A. Figure 10 shows the segmental volume fraction profiles of the phase-separated two-component homopolymer blend, across the channel. The system exhibits coexistence of two bulk phases A and B, and an interfacial region of finite width between them. Phase A has a majority of A-type homopolymers and a minority of B-type homopolymers. Phase B is just the opposite. The solid lines denote the equilibrium profiles (corresponding to time $t=0$). Upon equilibration, the system is sheared at the nominal shear rate $\dot{\gamma}=1\times10^{-3}\tau^{-1}$ until the steady state is achieved. The segmental volume fraction profiles at the nonequilibrium steady-state are represented by the symbols. At this shear rate, the nonequilibrium steady state profiles are not noticeably different from the equilibrium profiles. The short-range interactions between the polymer segments and the solid walls are neutral ($\chi_s=0$). For such interactions, the depletion of polymer

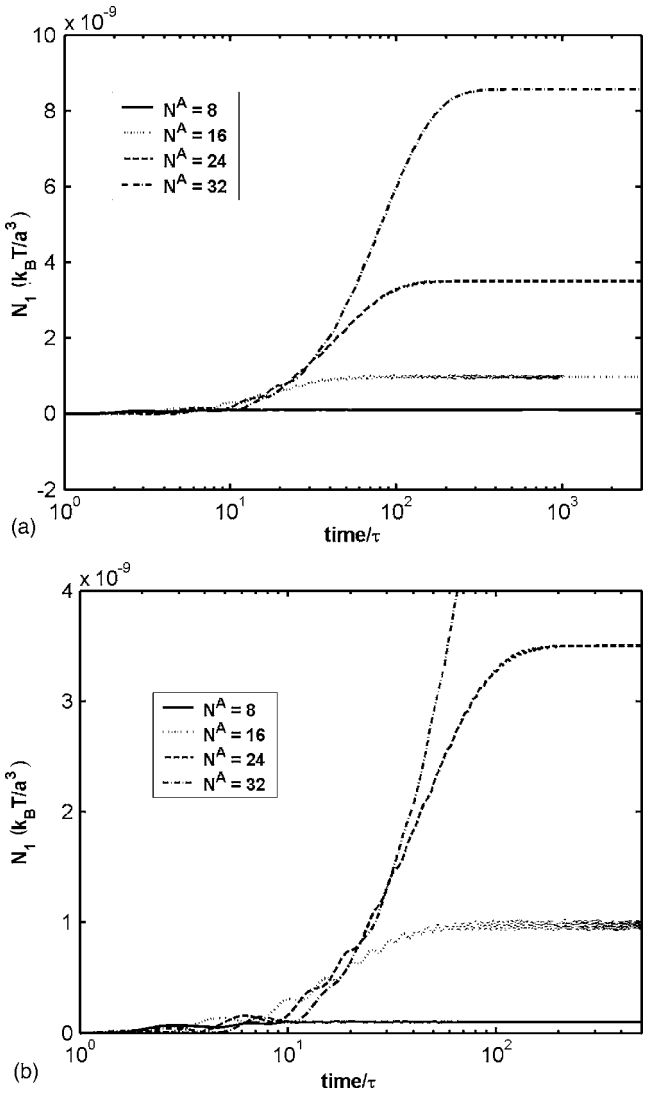

FIG. 9. (a) Time evolution of the first normal stress difference, $N_1=\sigma_{xx}-\sigma_{zz}$. The chain length varies from $N^A=8$ to 24. The other parameters are the same as in Fig. 4 with ($\chi_s=0$). (b) An enlarged view of the rise of the first normal stress difference.

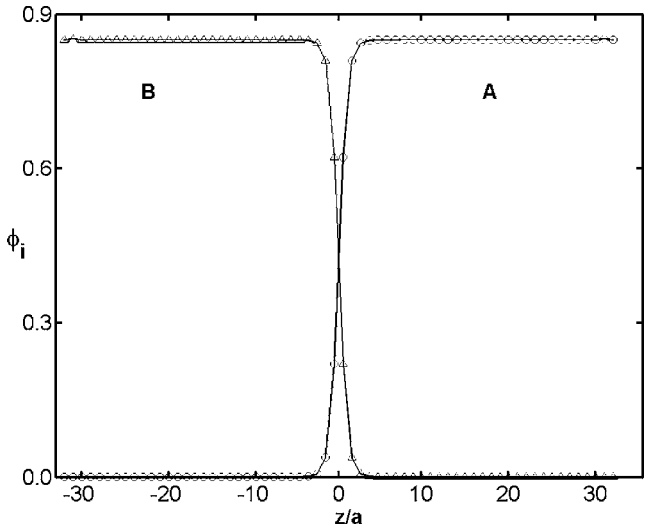

FIG. 10. Steady-state segmental volume fraction profiles of a two-component polymer blend, across the channel, obtained at a nominal shear rate $\dot{\gamma}=1\times10^{-3}\tau^{-1}$. Polymer chains consist of $N^A=N^B=24$ Kuhn segments. The segment-segment interaction parameter is $\chi_{AB}=0.55/12$ and the walls are neutral ($\chi_s=0$).

segments in the vicinity of the wall is slight on the scale shown.

Figure 11 displays the cross-channel variation of u_x, the x component of the mass-averaged steady-state velocity, centered about the polymer-polymer interface ($z=0$), obtained at a nominal shear rate $\dot{\gamma}=1\times10^{-3}\tau^{-1}$. There is a significant upward kink in the velocity profile in the interfacial region. This phenomenon is known as interfacial velocity slip. It can be quantified by the intercepts of the extrapolation of linear portion of the velocity profiles with the velocity axis (determining a velocity slip), or with the z axis normal to the interface (determining a slip length).

In Fig. 12, the variation of the shear viscosity across the interface is shown centered about the mid channel plane. The local shear viscosity decreases from the bulk values and

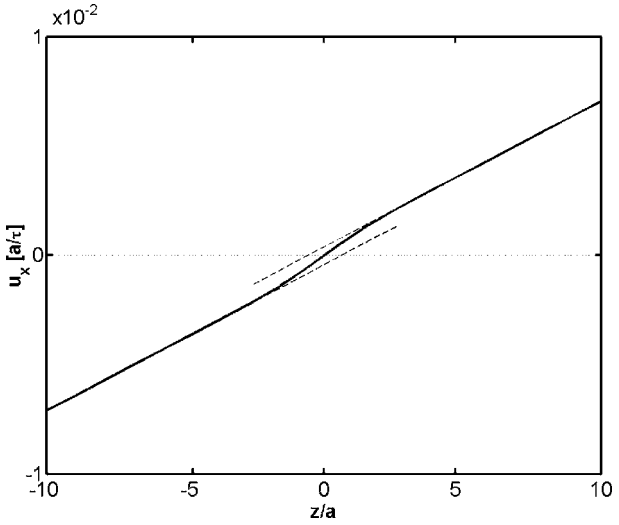

FIG. 11. Steady-state velocity profile, centered about the planar interface. Simulation parameters are the same as in Fig. 10.

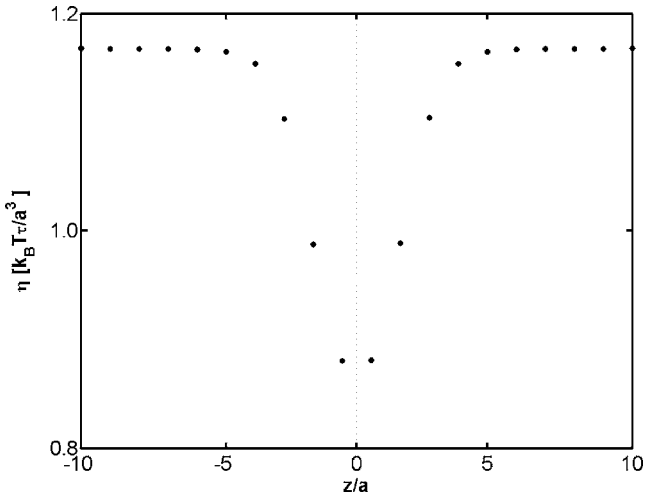

FIG. 12. Steady-state viscosity profile, centered about the interface of a phase-separated, two-component polymer blend. Simulation parameters are the same as in Fig. 10.

reaches a minimum at mid-channel. It is calculated by dividing the local shear stress, obtained from the local momentum density flux, by the local shear rate, obtained from the gradient of the velocity. The interfacial velocity slip and the accompanying reduction of shear viscosity across the interface have been first predicted based on scaling arguments [118,119]. More recently, it was analyzed [120] using numerical solutions of approximate constitutive equations for the evolution of the composition and of the deviatoric stress derived from the Rouse model assuming fluid incompressibility. Figures 11 and 12 are qualitatively similar to these predictions, as well as to results obtained by MD simulations [46,47] of the same phenomena. Similar phenomena have been observed experimentally [121–123], though the bulk

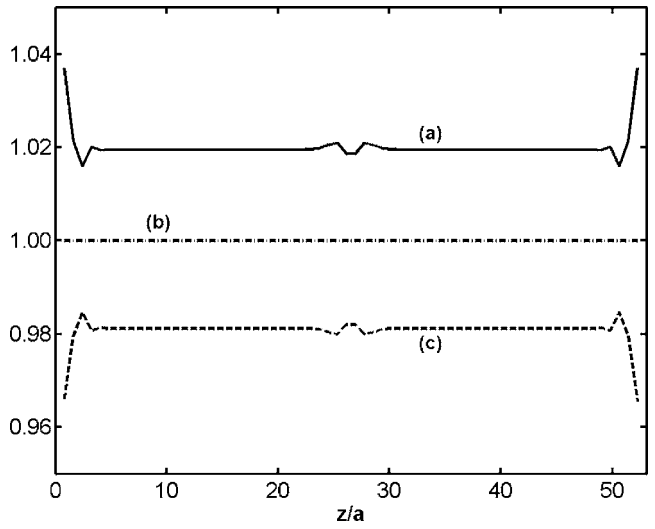

FIG. 13. Cross-channel stretching profile of an ideal (noninteracting) polymer test chain at the steady state. The stretching is calculated using the (a) largest, (b) intermediate, and (c) smallest eigenvalues of the second moment of the end-to-end distance, normalized by their values at equilibrium. Simulation parameters are the same as in Fig. 10.

phases of the observed polymer fluids were in the entangled regime.

The local stretching of an ideal (noninteracting) polymer test chain by nonuniform flows can be quantified by calculating the eigenvalues of the tensor of the second moment of the end-to-end vector for ideal chains, with their center of mass located at a particular layer. The three eigenvalues measure stretching along the three principal axes of this tensor. Fig. 13 shows the variation across the channel of the (a) largest, (b) intermediate, and (c) smallest eigenvalues at the steady state, normalized by their equilibrium values. At the nominal shear rate $\dot{\gamma}=1\times10^{-3}\tau^{-1}$, the strongest stretching ($\approx4\%$) occurs next to the walls, compared to $\approx2\%$ in the bulk phases. However, keep in mind that Fig. 13 displays stretching of an ideal (noninteracting) chain due to the nonuniform steady-state velocity profile. Note that chain stretching is affected by interfacial flows. The stretching shown in Fig. 13 does not account for segment-segment and segment-wall interactions. These are modeled by the interactions of segments with a self-consistent field as they perform random walks generating a chain configuration. The free segment and stepping probabilities obtained by numerical solutions of the DSCF evolution equations can be used to provide transition rates for Monte Carlo sampling of the second moment of the end-to-end distance of interacting chains. Such Monte Carlo DSCF calculations have been presented in a separate work [124].

VI. DISCUSSION

We have presented a lattice formulation for a DSCF theory for inhomogeneous fluids consisting of unentangled homopolymer chains between sheared parallel walls. It is based on probabilistic conservation laws for species occupancies and momentum that are coupled to models of polymer structure and conformation. Since the DSCF theory is formulated on the Kuhn length scale, it provides a computational method for resolving interfacial structure and dynamics at sheared interfaces with walls and between phase-separated domains. This was illustrated by DSCF simulations of transient and steady-state interfacial composition, flow, and rheology in unentangled, inhomogeneous polymer melts and blends.

Like any singlet-level mean field approach, the DSCF theory approximates the joint probability distribution of segments on a lattice by a product of one-body free segment probabilities at each site interacting with a local self-consistent potential field. Such an approximation underestimates many-body correlations and thermal fluctuations. These are enhanced as the equilibrium critical point for phase separation is approached, shifting the true critical temperature downward from its mean field value, and causing scaling crossover from the mean field to the three-dimensional Ising universality class in a narrow region about the critical point of a width characterized by the Ginzburg number Gi. Modeling the conformations of freely jointed chains as lattice random walks in a self-consistent field accounts for intrachain correlations imposed by the freely jointed chain constraint, but not for correlations propagated by interactions with adjacent segments and walls. The accuracy of equilibrium SCF theories for symmetric polymer blends increases with the chain length N, so that the mean field value for the critical point of a symmetric blend becomes asymptotically exact as $N\rightarrow\infty$. The mean field critical point $\chi=\chi_c$ satisfies $\chi_c N=2$ where $\chi=12\chi_{AB}$ is the Flory parameter related to χ_{AB}, the segment-segment interaction parameter on the fcc lattice that is used in our DSCF model. The leading correction causing the downward shift of the true critical temperature from its mean field value scales with chain length as $N^{-1/2}$, while the Ginzburg number Gi scales as N^{-1}. The current version of our DSCF theory is limited to unentangled polymers with $N<N_e\cong35$. For simulations of symmetric blends with chain length $N=24$ reported here, Gi is significantly smaller (by a factor of 0.04) than in a mixture of monomers, but the shift of the critical temperature from its mean field value is appreciable (assuming a pre-factor of order unity, the first order correction is about 20%). Application of shear further affects the critical fluctuations, the critical temperature shift, and the Ginzburg number Gi.

The DSCF simulations of sheared polymer blends reported here were done far from criticality, and hence are not affected by critical thermal fluctuations. However, our DSCF simulation neglects capillary thermal fluctuations, which are expected to broaden significantly the effective thickness of the interface between the two phases compared to the "intrinsic" DSCF interfacial profiles, such as those shown in Fig. 10. For a quantitative comparison of DSCF interfacial width with experimental observations or with MD and Monte Carlo simulations, it is necessary to account for such broadening of the "intrinsic" interface profile by using theoretical estimates of the capillary wave spectrum [125–128]. We report such a quantitative comparison of DSCF and MD interfacial profiles, accounting for capillary waves broadening, in a separate work [124].

The DSCF approach presented here can be generalized to account for different chain structure (e.g., block copolymers or branching) or for additional conservation laws and transport equations (e.g., for energy and/or charge). As any mean field theory, it can also be improved systematically by relaxing the factorization approximation for configurational probabilities, to account for joint probabilities of nearest-neighbor pairs, or of even larger compact clusters. For practical purposes, it is important to make it applicable to entangled polymer fluids. We have already succeeded in producing a crude version of a DSCF theory for inhomogeneous entangled polymer fluids. This was achieved by regarding reptation tube segments, rather than Kuhn segments, as the basic elements for our lattice DSCF model, and relating Larson's differential constitutive equation for tube segment orientation [8] (which is an approximation of the Doi-Edwards reputation theory [5]) to the evolution of the stepping probabilities used for modeling the primitive chain of the tube as a random walk in a self-consistent field under flow. However, this approach is limited to interfaces wider than the length scale of a tube segment. Resolution of interfacial dynamics of entangled polymers on the finer Kuhn length scale requires a more sophisticated approach. Work along these lines will be reported in future publications.

ACKNOWLEDGMENTS

We acknowledge numerous helpful discussions with Dr. Glen H. Ko, Dr. Stanislav Solovyov, Dr. Wentao Li, and Dr. Dilip Gersappe, for which we are very grateful. We thank Dr. Toshihiro Kawakatsu for sending us a copy of [37] summarizing the relevant work of his group prior to its publication. This work was initiated while the authors were at the Department of Chemical Engineering and Chemistry at the Polytechnic University in Brooklyn, NY. Some preliminary results were included in [129]. M.M. and Y.S. thank the National Science Foundation for financial support (Grant No. DMR-0080604). T.S.L. and Y.S. acknowledge a grant from the Mitsubishi Chemical Corporation of Japan, for which they are grateful.

[1] H. Eyring, J. Chem. Phys. **4**, 283 (1936).
[2] J. I. Frenkel, *Kinetic Theory of Liquids* (Oxford University Press, Oxford, 1946).
[3] A. A. Khan and Y. Shnidman, Prog. Colloid Polym. Sci. **103**, 251 (1997).
[4] A. A. Khan, Ph.D. Thesis, University of Rochester, Rochester, NY, 1999 (unpublished).
[5] M. Doi and S. F. Edwards, *The Theory of Polymer Dynamics* (Oxford University Press, Oxford, 1986).
[6] R. B. Bird, C. F. Curtiss, R. C. Armstrong, and O. Hassager, *Dynamics of Polymeric Liquids* 2nd edition (Wiley, New York, 1987, Vol. 2).
[7] A. Y. Grosberg and A. R. Khokhlov, *Statistical Physics of Macromolecules* (AIP Press, New York, 1994).
[8] R. G. Larson, *Constitutive Equations for Polymer Melts and Solutions* (Butterworths, Boston, 1988).
[9] R. G. Larson, *The Structure and Rheology of Complex Fluids* (Oxford University Press, Oxford, 1999).
[10] D. Jou, J. Casas-Vasquez, and M. Criado-Sancho, *Thermodynamics of Fluids under Flow* (Springer, Berlin, 2001).
[11] J. F. Gouyet, M. Plapp, W. Dieterich, and P. Maass, Adv. Phys. **52**, 523 (2003).
[12] J. M. H. M. Scheutjens and G. J. Fleer, J. Phys. Chem. **83**, 1619 (1979).
[13] H. R. Warner, Jr., Ph.D. Thesis University of Wisconsin, 1971 (unpublished)).
[14] H. R. Warner, Jr., Ind. Eng. Chem. Fundam. **11**, 379 (1972).
[15] R. C. Armstrong, J. Chem. Phys. **60**, 724 (1974).
[16] A. Peterlin, Makromol. Chem. **338**, 44 (1961).
[17] A. Peterlin, Kolloid Z. Z. Polym. **182**, 110 (1962).
[18] M. Herrchen and H. C. Ottinger, J. Non-Newtonian Fluid Mech. **68**, 17 (1997).
[19] S. F. Edwards, Proc. Phys. Soc. London **85**, 613 (1965).
[20] E. Helfand and Y. Tagami, J. Chem. Phys. **56**, 3592 (1972).
[21] A. K. Dolan and S. F. Edwards, Proc. R. Soc. London, Ser. A **337**, 509 (1974).
[22] F. Schmid, J. Phys.: Condens. Matter **10**, 8105 (1998).
[23] K. Kawasaki and K. Sekimoto, Physica A **143**, 349 (1987).
[24] J. G. E. M. Fraaije, J. Chem. Phys. **99**, 9202 (1993).
[25] J. G. E. M. Fraaije, B. A. C. van Vlimmeren, N. M. Maurits, M. Postma, O. A. Evers, C. Hoffmann, P. Altevogt, and G. GoldbeckWood, J. Chem. Phys. **106**, 4260 (1997).
[26] N. M. Maurits, B. A. C. van Vlimmeren, and J. G. E. M. Fraaije, Phys. Rev. E **56**, 816 (1997).
[27] N. M. Maurits and J. G. E. M. Fraaije, J. Chem. Phys. **107**, 5879 (1997).
[28] A. V. Zvelindovsky, G. J. A. Sevink, B. A. C. van Vlimmeren, N. M. Maurits, and J. G. E. M. Fraaije, Phys. Rev. E **57**, R4879 (1998).
[29] R. Hasegawa and M. Doi, Macromolecules **30**, 3086 (1997).
[30] R. Hasegawa and M. Doi, Macromolecules **30**, 5490 (1997).
[31] K. Furuichi, C. Nonomura, T. Kawakatsu, and M. Doi, J. Chem. Phys. **117**, 9959 (2002).
[32] T. Kawakatsu, Phys. Rev. E **56**, 3240 (1997).
[33] H. Morita, T. Kawakatsu, and M. M. Doi, Macromolecules **34**, 8777 (2001).
[34] H. Morita, T. Kawakatsu, M. Doi, D. Yamaguchi, M. Takenaka, and T. Hashimoto, Macromolecules **35**, 7473 (2002).
[35] N. M. Maurits, A. V. Zvelindovsky, and J. G. E. M. Fraaije, J. Chem. Phys. **108**, 2638 (1998).
[36] N. M. Maurits, A. V. Zvelindovsky, and J. G. E. M. Fraaije, J. Chem. Phys. **109**, 11032 (1998).
[37] T. Shima, H. Kuni, Y. Okabe, M. Doi, H. F. Yuan, and T. Kawakatsu, Macromolecules **36**, 9199 (2003).
[38] A. N. Beris and B. J. Edwards, *Thermodynamics of Flowing Systems with Internal Microstructure* (Oxford University Press, Oxford, 1994).
[39] M. Grmela and H. C. Ottinger, Phys. Rev. E **56**, 6620 (1997).
[40] H. C. Ottinger and M. Grmela, Phys. Rev. E **56**, 6633 (1997).
[41] V. G. Mavrantzas and A. N. Beris, J. Chem. Phys. **110**, 616 (1999).
[42] V. G. Mavrantzas and A. N. Beris, J. Chem. Phys. **110**, 628 (1999).
[43] K. Binder, *Monte Carlo and Molecular Dynamics Simulations in Polymer Science* (Oxford University Press, Oxford, 1995).
[44] K. Kremer and G. S. Grest, J. Chem. Phys. **92**, 5057 (1990).
[45] W. Paul, G. D. Smith, D. Y. Yoon, B. Farago, S. Rathgeber, A. Zirkel, L. Willner, and D. Richter, Phys. Rev. Lett. **80**, 2346 (1998).
[46] S. Barsky and M. O. Robbins, Phys. Rev. E **63**, 021801 (2001).
[47] S. Barsky and M. O. Robbins, Phys. Rev. E **65**, 021808 (2002).
[48] M. Lasso and H. C. Ottinger, J. Non-Newtonian Fluid Mech. **47**, 1 (1993).
[49] V. Ganesan and V. Pryamitsyn, J. Chem. Phys. **118**, 4345 (2003).
[50] P. J. Hoogerbrugge and J. M. V. A. Koelman, Europhys. Lett. **19**, 155 (1992).
[51] J. M. V. A. Koelman and P. J. Hoogerbrugge, Europhys. Lett. **21**, 363 (1993).
[52] Y. Kong, C. W. Manke, W. G. Madden, and A. G. Schlijper, Int. J. Thermophys. **15**, 1093 (1994).
[53] A. G. Schlijper, P. J. Hoogerbrugge, and C. W. Manke, J.

Rheol. **39**, 567 (1995).
[54] P. Espanol and P. B. Warren, Europhys. Lett. **30**, 191 (1995).
[55] R. D. Groot and P. B. Warren, J. Chem. Phys. **107**, 4423 (1997).
[56] R. Zwanzig, Phys. Rev. **124**, 983 (1961).
[57] H. C. Ottinger, Phys. Rev. E **57**, 1416 (1998).
[58] M. Doi and A. Onuki, J. Phys. II **2**, 1631 (1992).
[59] S. T. Milner, Phys. Rev. E **48**, 3674 (1993).
[60] B. C. Eu, *Kinetic Theory and Irreversible Thermodynamics* (Wiley, New York, 1992).
[61] G. H. Fredrickson, J. Chem. Phys. **117**, 6810 (2002).
[62] P. M. Chaikin and T. C. Lubensky, *Principles of Condensed Matter Physics* (Cambridge University Press, Cambridge, U.K., 1995).
[63] N. W. Ashcroft and N. D. Mermin, *Solid State Physics* (Harcourt Brace, New York, 1976).
[64] T. D. Lee and C. N. Yang, Phys. Rev. **87**, 410 (1952).
[65] P. J. Flory, J. Chem. Phys. **10**, 51 (1942).
[66] M. L. Huggins, J. Phys. Chem. **46**, 151 (1942).
[67] P. J. Flory, *Principles of Polymer Chemistry* (Cornell University Press, Ithaca, NY, 1953).
[68] J. Scheutjens and G. J. Fleer, J. Phys. Chem. **83**, 1619 (1979).
[69] D. N. Theodorou, J. Chem. Phys. **22**, 4578 (1989).
[70] D. N. Theodorou, Macromolecules **22**, 4589 (1989).
[71] A. Hariharan, S. K. Kumar, and T. P. Russell, J. Chem. Phys. **99**, 4041 (1993).
[72] W. L. Bragg and E. J. Williams, Proc. R. Soc. London, Ser. A **145**, 699 (1934).
[73] W. L. Bragg and E. J. Williams, Proc. R. Soc. London, Ser. A **151**, 540 (1935).
[74] W. L. Bragg and E. J. Williams, Proc. R. Soc. London, Ser. A **152**, 231 (1935).
[75] S. Chen and G. D. Doolan, Annu. Rev. Fluid Mech. **30**, 329 (1998).
[76] E. Orlandini, M. R. Swift, and J. M. Yeomans, Europhys. Lett. **32**, 463 (1995).
[77] M. R. Swift, E. Orlandini, W. R. Osborn, and J. M. Yeomans, Phys. Rev. E **54**, 5041 (1996).
[78] A. Malevanets and J. M. Yeomans, Faraday Discuss. **112**, 237 (1999).
[79] N. S. Martys and J. F. Douglas, Phys. Rev. E **63**, 031205 (2001).
[80] J. W. Cahn and J. E. Hilliard, J. Chem. Phys. **28**, 258 (1958).
[81] H. E. Cook, Acta Metall. **18**, 297 (1970).
[82] P. C. Hoenberg and B. I. Halperin, Rev. Mod. Phys. **49**, 435 (1977).
[83] R. A. L. Jones and R. W. Richards, *Polymers at Surfaces and Interfaces* (Cambridge University Press, Cambridge, U.K., 1999).
[84] P. G. de Gennes, *Scaling Concepts in Polymer Physics* (Cornell University Press, Ithaca, NY, 1979).
[85] N. G. Van Kampen, *Stochastic Processes in Physics and Chemistry* (North-Holland, Amsterdam, 1992).
[86] G. H. Weiss, *Aspects and Applications of the Random Walk* (North-Holland, Amsterdam, 1994).
[87] I. C. Sanchez and R. H. Lacombe, J. Phys. Chem. **80**, 2352 (1976).
[88] I. C. Sanchez and R. H. Lacombe, Macromolecules **11**, 1145 (1978).
[89] O. A. Evers, J. Scheutjens, and G. J. Fleer, J. Chem. Soc., Faraday Trans. **86**, 1333 (1990).
[90] P. E. Rouse, J. Chem. Phys. **21**, 1272 (1953).
[91] H. Giesekus, Rheol. Acta **1**, 2 (1958).
[92] A. S. Lodge, Rheol. Acta **10**, 539 (1971).
[93] K. Kawasaki, Phys. Rev. **145**, 224 (1966).
[94] K. Kawasaki, in *Phase Transitions and Critical Phenomena*, edited by C. Domb and M. S. Green (Academic Press, New York, 1972), Vol. 2.
[95] B. Schmittmann and R. K. P. Zia, *Statistical Mechanics of Driven Diffusive Systems* (Academic Press, London, 1995).
[96] K. Binder, *Monte Carlo Methods in Statistical Physics* (Springer, Berlin, 1986).
[97] J. W. Cahn, J. Chem. Phys. **66**, 3667 (1977).
[98] G. J. Fix, in *Free Boundary Problems: Theory and Applications* edited by A. Fasano and M. Primicerio (Piman, Boston, 1983), p. 580.
[99] J. S. Langer, in *Directions in Condensed Matter Physics*, edited by G. Grinstein, and G. Mazenko (World Scientific, Singapore, 1986).
[100] M. Suzuki and R. Kubo, J. Phys. Soc. Jpn. **24**, 51 (1968).
[101] K. Binder, Z. Phys. **267**, 313 (1974).
[102] S. Katz, J. L. Lebowitz, and H. Spohn, J. Stat. Phys. **34**, 497 (1984).
[103] A. K. Doolittle and D. B. Doolittle, J. Appl. Phys. **28**, 901 (1957).
[104] H. Vogel, Phys. Z. **22**, 645 (1921).
[105] G. S. Fulcher, J. Am. Chem. Soc. **8**, 339 (1925).
[106] G. S. Fulcher, J. Am. Chem. Soc. **8**, 789 (1925).
[107] G. Tammann and G. Hesse, Z. Anorg. Allg. Chem. **156**, 245 (1926).
[108] M. L. Williams, R. F. Landel, and J. D. Ferry, J. Am. Chem. Soc. **77**, 3701 (1955).
[109] J. Ferry, *Viscoelastic Properties of Polymers* (Wiley, New York, 1980).
[110] B. Q. Li and E. Ruckenstein, J. Chem. Phys. **106**, 280 (1997).
[111] M. Putz, K. Kremer, and G. S. Grest, Europhys. Lett. **49**, 735 (2000).
[112] Y. J. A. Mochimaru, J. Non-Newtonian Fluid Mech. **12**, 135 (1983).
[113] R. J. LeVeque, *Numerical Methods for Conservation Laws* (Birkhauser, Basel, 1992).
[114] D. M. Tolstoi, Dokl. Akad. Nauk SSSR **85**, 1089 (1952).
[115] T. D. Blake, Colloids Surf. **47**, 135 (1990).
[116] E. Ruckenstein and N. Churayev, J. Colloid Interface Sci. **147**, 535 (1991).
[117] A. A. Alexeyev and O. I. Vinogradova, Colloids Surf., A **108**, 173 (1996).
[118] P. G. de Gennes, C. R. Acad. Sci., Ser. II: Mec., Phys., Chim., Sci. Terre Univers **308**, 1401 (1989).
[119] F. Brochard-Wyart, P. G. de Gennes, and S. Troian, C. R. Acad. Sci., Ser. II: Mec., Phys., Chim., Sci. Terre Univers **310**, 1169 (1990).
[120] J. L. Goveas and G. H. Fredrickson, Eur. Phys. J. B **2**, 79 (1998).
[121] R. Zhao and C. W. Macosko, J. Rheol. **46**, 145 (2002).
[122] Y. C. Lam, L. Jiang, C. Y. Yue, K. C. Tam, L. Li, and X. Hu, J. Rheol. **47**, 795 (2003).
[123] Y. C. Lam, C. Y. Yue, Y. X. Yang, K. C. Tam, and X. Hu, J. Appl. Polym. Sci. **87**, 258 (2003).
[124] T. S. Lo, M. Mihajlovic, Y. Shnidman, W. T. Li, and D. Ger-

sappe, this issue, Phys. Rev. E **72** 040801(R) (2005).
[125] A. N. Semenov, Macromolecules **27**, 2732 (1994).
[126] A. Werner, F. Schmid, M. Muller, and K. Binder, J. Chem. Phys. **107**, 8175 (1997).
[127] M. D. Lacasse, G. S. Grest, and A. J. Levine, Phys. Rev. Lett. **80**, 309 (1998).
[128] K. Binder, M. Muller, F. Schmid, and A. Werner, Adv. Colloid Interface Sci. **94**, 237 (2001).
[129] M. Mihajlovic, Ph.D. Thesis, Polytechnic University, Brooklyn, 2004 (unpublished).